AD-A053 067 AIR FORCE GEOPHYSICS LAB HANSCOM AFB MASS F/G 17/9
SHORT ARC REDUCTION OF RADAR ALTIMETRY COMPUTER PROGRAM.(U)
JAN 78 G HADGIGEORGE, J TROTTER NASA-P-57270(6)
UNCLASSIFIED AFGL-TR-77-0170 NASA-CR-141434 NL

END
DATE FILMED
6 -78
DDC

(14) AFGL-TR-77-0170

(2)

(18) (9) (19) NASA CONTRACTOR REPORT CR-141434

(6)

Short Arc Reduction Of Radar Altimetry Computer Program

(10) George Hadgigeorge
and
Jerry Trotter

(15) NASA-P-5727 (G)

(11) Jan 1978

(12) 90 p.

National Aeronautics and
Space Administration

Wallops Flight Center
Wallops Island, Virginia 23337
AC 804 824-3411

409 578

NASA CONTRACTOR REPORT 141434

Short Arc Reduction Of Radar Altimetry Computer Program

George Hadgigeorge
and
Jerry Trotter

Air Force Geophysics Laboratory
Air Force Systems Command
United States Air Force
Hanscom AFB, Massachusetts 01731

Prepared under Purchase Order No. P-57270 (G)

National Aeronautics and
Space Administration

Wallops Flight Center
Wallops Island, Virginia 23337
AC 804 824-3411

TABLE OF CONTENTS

SECTION	DESCRIPTION	PAGE
1	BACKGROUND	1
2	INTRODUCTION TO SHORT ARC APPLICATION TO REGIONAL GEOID REDUCTIONS	4
3	INVESTIGATIVE EXPERIMENTS CONDUCTED TO DETERMINE THE FEASIBILITY OF THE SHORT ARC APPROACH	8
	3.1 Preliminary Exercises of the Spheroidal Multiquadric Model	9
	3.2 Computer Simulation of the Recovery of Geoidal Undulation Over the North Atlantic	14
	3.3 *Reductions of First Available* Satellite Altimetric Data from Skylab	20
	3.4 Preliminary Reduction of GEOS-3 Altimetric Data Over the North Atlantic	27
	3.4.1 Unknowns and Constraints Used in the Reduction	28
	3.4.2 Results	29
4	MATHEMATICAL SURFACE MODELS	35
	4.1 Uses of the Covariance Function in SARRA	35
	4.2 Spheroidal Multiquadric Surface Model	37
5	FORMATION AND SOLUTION OF NORMAL EQUATIONS	39
6	ANALYSIS OF RESIDUALS	45

SECTION	DESCRIPTION	PAGE
7	FINAL RESULTS OF GEOID SURFACES DETERMINED BY THE SHORT ARC APPROACH UTILIZING ALL AVAILABLE DATA	50
	7.1 Unknowns and Constraints Used in the Reductions	50
	7.2 Reduction Results	51
	7.3 Residual and Profile Analysis	56
8	PRE AND POST PROCESSING AUXILIARY PROGRAMS FOR SARRA REDUCTIONS OF SATELLITE ALTIMETRY DATA	66
	8.1 Pre-processor	66
	8.2 Post SARRA Plot Programs	70
APPENDIX A		73
	REFERENCES	82

LIST OF FIGURES

FIGURE NO.	DESCRIPTION	PAGE
1	Illustrating ground tracks of every fifth pass of approximately 200 passes of GEOS-C considered in hypothetical short arc determination of fine structure of North Atlantic geoid.	6
2	Map showing countours of Gravimetric Geoid and locations of selected nodes employed in preliminary testing of the Spheroidal Multiquadric Model.	11
3	RMS fit - Grid level - Nodal density.	12
4	Contour interval - RMS residual.	13
5	Illustration of the simulation of 200 satellite passes that are approximately over the North Atlantic Oceanic region.	16
6	Illustration of the simulation of 320 satellite passes that are approximately over the North Atlantic Oceanic region.	17
7	Skylab ground tracks.	21
8	Skylab altimeter data pass #4.	23
9	Skylab altimeter data pass #4 - Puerto Rico Trench only.	24
10	Comparison of Gravimetric Geoid with Skylab altimeter data.	25
11	Skylab altimeter data pass #9.	26
12	Calibration area GEOS-3 ground tracks.	30
13	Geoid contour map of the GEOS-3 calibration area.	31
14	Comparison of GEOS-3 derived Geoid and NASA Calibration Area Gravimetric Geoid.	33
15	Comparison of GEOS-3 derived Geoid and NASA Calibration Area Gravimetric Geoid.	34

LIST OF FIGURES (*continued*)

FIGURE NO.	DESCRIPTION	PAGE
16	Ground track of satellite passes over the North Atlantic Ocean.	52
17	Geoid contour produced by the reduction use of the Covariance Function Surface Model.	54
18	Geoid contour produced by the reductions using the Multiquadric Analysis for the Surface Model.	55
19	Residuals from pass 2531413.	57
20	Residuals from pass 1222133.	58
21	Residuals from pass 3040601.	59
22	Geoid profile along pass 2531413 using Multiquadric Surface Model.	60
23	Geoid profile along pass 2531413 using the Covariance Function Surface Model.	61
24	Geoid profile along pass 1222133 using the Multiquadric Surface Model.	62
25	Geoid profile along pass 1222133 using the Covariance Function Surface Model.	63
26	Geoid profile along pass 3040601 using the Multiquadric Surface Model.	64
27	Geoid profile along pass 3040601 using the Covariance Function Surface Model.	65
28	North Atlantic data rejection limits.	72

LIST OF TABLES

TABLE NO.	DESCRIPTION	PAGE
1	Basic assumptions underlying various simulations.	18
2	Key results of simulations.	19

SECTION 1

BACKGROUND

In 1970, AFGL contracted DBA Systems to perform a study of various reduction approaches to satellite altimetric measurements of the oceanic geoid surface. This study was initiated in view of the then upcoming launch of the GEOS-3 Satellite which was designed to carry a radar altimeter. The primary objective was to derive alternative reduction approaches that may remove the necessity for extremely accurate reference orbits of GEOS-3 required by conventional approaches.

Conventional approaches to the reduction of satellite altimeter data utilize long arc orbit integration that requires extensive tracking from ground based trackers to maintain extremely accurate orbits. A widely held premise was that in order to exploit the satellite altimeter of 1 meter accuracy for geoid improvement, it was necessary that the radial component of satellite position be known to better then $\pm$ 1 meter. An example is extracted from reference 11 that states "Because the orbit will be used in combination with altimeter measurements in the data reduction process leading to geoid improvement, it is necessary that the accuracy in S/C height as calculated from the orbit be known to better than $\pm$ 1 meter". Problems arose that made the above requirement very difficult. Among these problems are (a) *unresolved biases in a given tracker could induce*

localized systematic errors in the computed orbit which could be transferred to the local geoid, (b) *unmodeled perturbations caused by drag radiation pressure,* (c) *errors in long arc orbits result from integrated effects of errors in the adopted geopotential function* and (d) *most important is the extensive effort and cost of global tracking networks and computer processing required to provide such accurate reference orbits.*

In view of the above difficulties, our investigation was directed toward alternative approaches that would fully exploit the 1 meter altimeter accuracy for geoid determination with less stringent requirements for orbital accuracies. This led to the investigation of the feasibility of utilizing the short arc technology that AFGL/DBA had developed in previous satellite geodesy programs. Such an approach was envisioned to involve the simultaneous recovery of state vectors defining as many as several thousand short arcs (subject to weak or prior constraints) along with the mathematical model used to define the geoid surface. The estimated orbit accuracy requirement was $\pm$ 100 meters, which is easily attainable from routine global tracking.

The short arc approach is defined as orbital arcs no greater than one fourth revolution. It was shown in *Brown (1967)*

that accuracies of integration of better than 1 meter can be attained in short arc reductions provided that

a) *spherical harmonies at least through* $(n,m) = (4,4)$ *are exercised in the integration*

and

b) *all six orbital parameters* $(X_0, Y_0, Z_0, \dot{X}_0, \dot{Y}_0, \dot{Z}_0)$ *at mid-arc are free to adjust to best accommodate the actual orbit.*

SECTION 2

INTRODUCTION OF THE SHORT ARC APPLICATION TO REGIONAL GEOID REDUCTIONS

The initial investigation established that the short arc approach was feasible and offered a flexible means of utilizing altimeter data for determining the geoid surface for a wide range of applications. The initial consideration of the short arc method employed spherical harmonics to mathematically define the geoid surface. This development is well suited to global representations of the geoid undulations and has been implemented into a computer program (*SAGG*) for the combination of Satellite Altimetry and Ground Gravity reduction. However, it was anticipated that the early data collection phase of the GEOS-3 program would concentrate on altimeter measurements over the North Atlantic calibration area. Additionally, it was felt that investigations of fine detail over limited localized regions would require an extravagant spherical harmonic expression. Therefore, alternative means for analytical representation of the geoid surface were explored. The most suitable model for the proposed application was a derivation of the spheroidal multiquadric analysis developed by *Hardy (1972)*. In Hardy's exercise of the multiquadric analysis, the nodes (*coefficient computation point*) correspond to observed data points. In our derivation, the nodes do not necessarily correspond to data points, are relatively limited in number and, at the outset, are evenly distributed.

The primary objective of this project was the short arc determination of the North Atlantic geoid, utilizing the spheroidal multiquadric analysis. This led to the development of the computer program SARRA (*Short Arc Reduction of Radar Altimetry*). It was envisioned that the altimeter observation would cover the entire North Atlantic Ocean at spacings of approximately a 1^0 by 1^0 grid with an initial selection of nodal points at 5^0 by 5^0 grid as illustrated by Figure 1.

As data became available, it was evident that there was a high concentration of the observations over the calibration area with sparse measurements over the northeastern portion of the North Atlantic Ocean and almost none in the southeastern portion. The results of the reduction indicated a close detailed agreement of the dense data area with other geoid models (*Marsh, Vincent, Strange*), but the geoid in the sparse areas (*northeastern*) seemed tilted toward the more dense areas. This geoid behavior caused concern with the use of the multiquadric analysis when the data is non-uniform and sparse in certain areas. Consequently, other possible surface models were investigated.

Upon suggestions by *Dr. Donald Eckhart (AFGL)** and extensive theoretical investigation by *Dr. George Blaha (DBA)***, the use of the covariance function was introduced as a second option to the computer program SARRA. The two options now offer flexibility depending on the characteristics of the available data. Both options are demonstrated

---

* *Air Force Geophysics Laboratory, LGHanscom Air Force Base, Ma. Personal communication.*

** *DBA Systems, Inc., Melbourne, FL. Personal communication.*

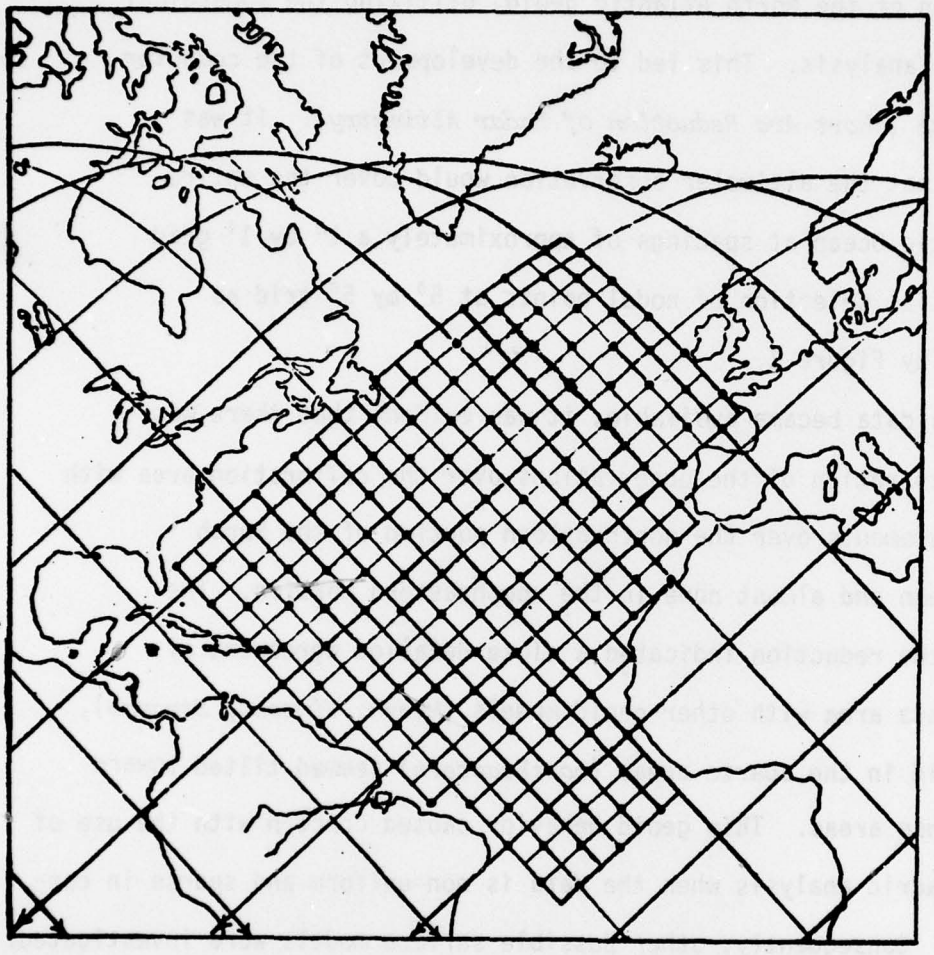

FIGURE 1. Illustrating ground tracks of every fifth pass of approximately 200 passes of GEOS C considered in hypothetical short arc determination of fine structure of North Atlantic geoid. Indicated tracks generate approximate $5^0 \times 5^0$ cells. Selected nodes for initial representation of North Atlantic geoid by means of spheroidal multiquadric functions are located nominally at alternate corners of $5^0 \times 5^0$ cells as indicated by solid dots. Initial set of approximately 150 nodes is subsequently to be augmented by additional nodes at locations indicated by residuals from initial reductions.

in the results portion of this report. Details of the multiquadric analysis and the covariance function models are presented in Section 4.1 of this report. The covariance function that is implemented into SARRA refers to a chosen reference ellipsoid.

The advantage of the covariance function is realized when data is irregularly distributed with some surface areas being very sparse in measurements. The covariance function implies some *apriori* knowledge of the geoid behavior through the spherical harmonic coefficients. The spheroidal multiquadric analysis is completely dependent on observation data and reproduces a surface model as the best least squares fit of the observation data. The advantage of using the multiquadric analysis model is realized when the area to be processed is covered with an adequately dense set of altimeter measurements. One unique feature of the multiquadric analysis is that there is essentially no limit on the size of the area to be processed and, provided enough data, one can obtain as much detail as the data provides by the proper selection of nodal points.

SECTION 3

INVESTIGATIVE EXPERIMENTS CONDUCTED TO DETERMINE THE FEASIBILITY OF THE SHORT ARC APPROACH

In the development of the computer program SARRA, a series of investigations were conducted for the purposes of determining

a) *the basic feasibility of the application of the short arc technology to geoid recovery from satellite altimetry,*

b) *the most suitable math models for representing the geoid surface in regard to the intended application,*

c) *testing the overall concept with simulation for its ultimate accuracy potential,*

d) *formulation of the overall concept into a reduction program capable of routinely processing the observation data when GEOS-3 became operational*

and

e) *develop auxiliary programs for the pre and post processing required in an operational environment.*

The key steps in this investigation are summarized in this section. However, the full detail may be found in references 1 and 11.

It was surmised in *Brown (1973)* that the spheroidal multiquadratic model would be well suited to detailed representation of the geoidal surface over such local regions as the North Atlantic (*where intensive testing of GEOS-C was to be conducted*).

In such applications, the model has the virtue of relative simplicity and is especially attractive in the flexibility afforded by the process referred to as *nodal densification*. This is an adaptive process wherein the original set of regularly spaced nodes (*defining the multiquadric function*) are supplemented locally as needed to improve the fit over irregular areas inadequately modeled at the outset.

Despite its theoretical attractiveness, the spheroidal multiquadric model had to be implemented and tested. The next section outlines the measures taken in evaluating the model under a well controlled experiment with data typical of geoid features.

3.1 Preliminary Exercises of the Spheroidal Multiquadric Model

In order to ascertain the basic adequacy of the spheroidal multiquadric model, two preliminary numerical tests were performed. The first test was to determine if the model was inherently capable of providing a reasonably good fit to the geoid; the second was to test the model as incorporated in SARRA with extensive simulations. These simulations will be presented in the next section(Section 3.2).

The first test used as a data base, the gravimetric geoid of a portion of the North Atlantic produced by *Marsh, Strange* and *Vincent* (*1972*). A sample of about 250 spot elevations of the geoid were extracted from the contour map of this geoid. These geoidal heights were treated as if they were direct observations.

The multiquadric model was then fitted by least squares to this data set using an initial set of 112 nodes spaced at five degree intervals (see Figure 2). The process of nodal densification was invoked in three iterations of the adjustment to introduce fresh nodes in regions leading initially to residuals in excess of two meters. This led ultimately to the incorporation of 22 additional nodes, several of which were in the region of the severe undulation over the Puerto Rico Trench. The final rms error of the fit of the multiquadric model turned out to be an altogether acceptable 0.75 m (*the precision of the digitization of the contour map was deemed to be not much better than 0.5 m*). This test established two things:

(a) *that the spheroidal multiquadratic function could provide an accurate representation of regional undulations of the geoid,*

and

(b) *that the process of nodal densification provides a valid, effective and efficient means for extending the model as needed for local improvement of fit.*

Figure 3 is the contour produced by the reduction and Figure 4 represents contour of closeness of fit.

With the fundamental soundness of the spheroidal multiquadric model firmly established as a result of the first preliminary test, steps were taken to incorporate the model into SARRA. After the revised program had been checked out on DBA's Xerox Sigma 5 computer, a small scale simulation was performed to provide a

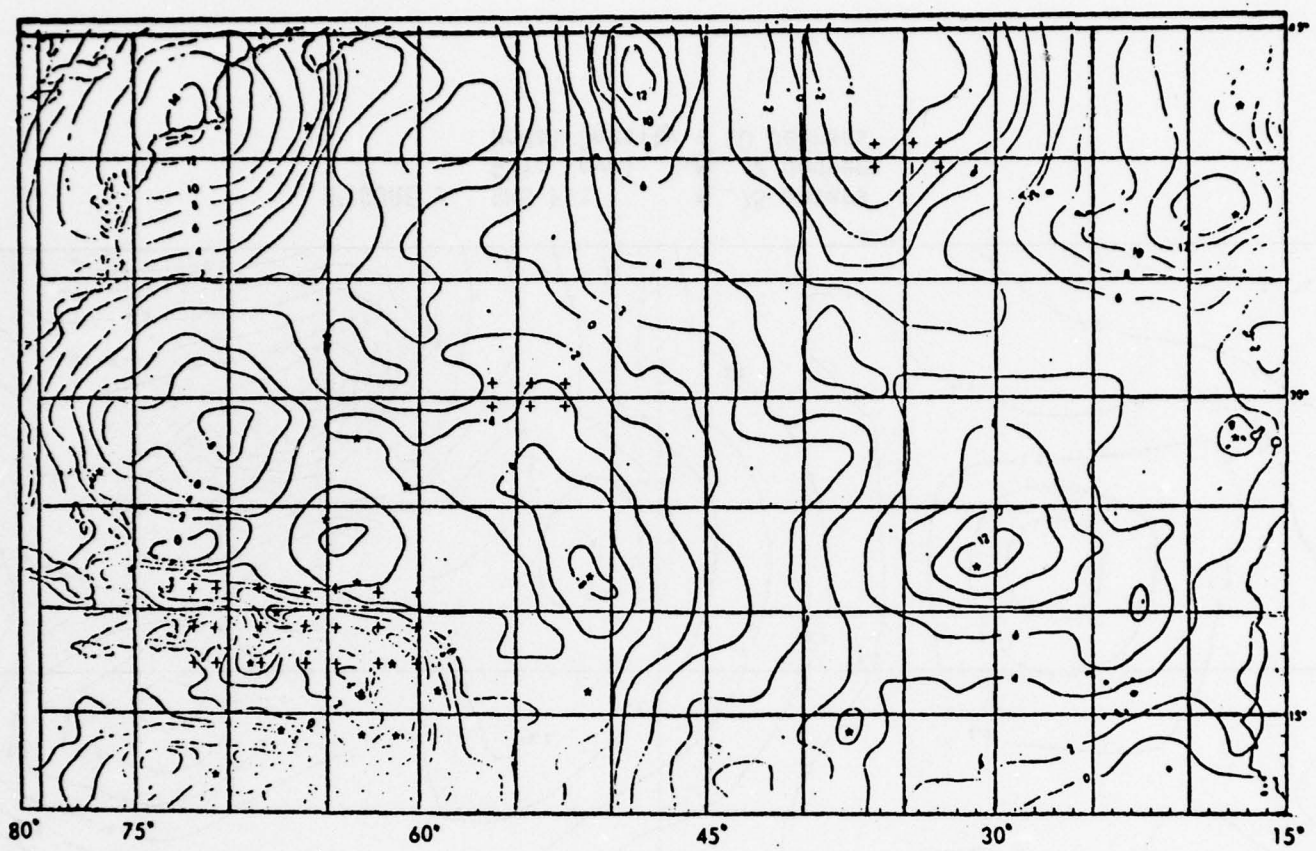

• Supplementary nodes
+ Supplementary Data

The initial node selection is represented by the intersection of the grid lines of figure. The initial data was interpolated at each 2° grid starting at latitude 17° and longitude 15° west through latitude 44° and longitude 79° west.

FIGURE 2. Map Showing Contours of Gravimetric Geoid and Locations of Selected Nodes Employed in Preliminary Testing of the Spheroidal Multiquadric Model

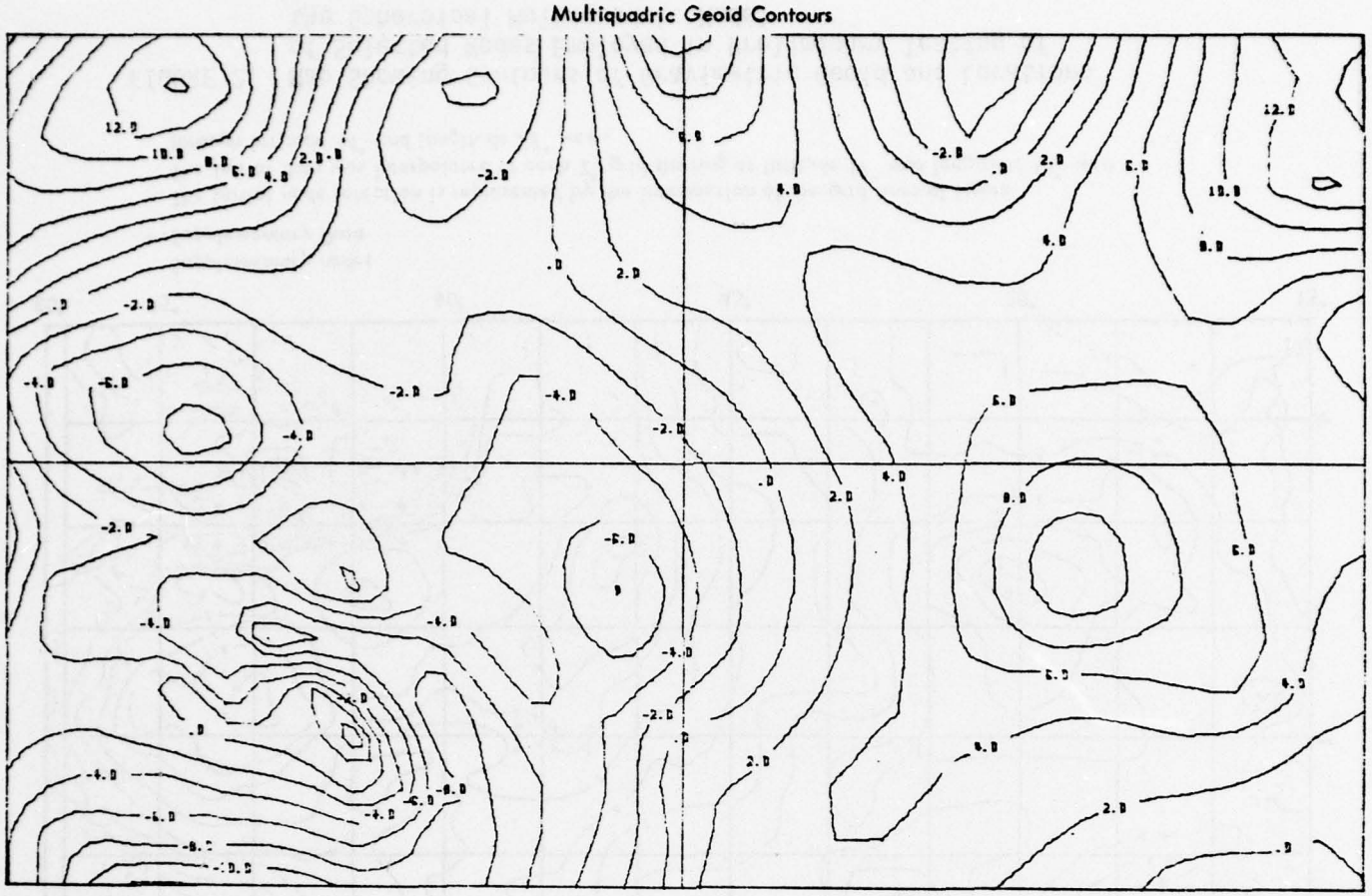

FIGURE 3. RMS Fit = .75 meters
Grid Level = 2 degrees
Nodal Density = 10 degrees

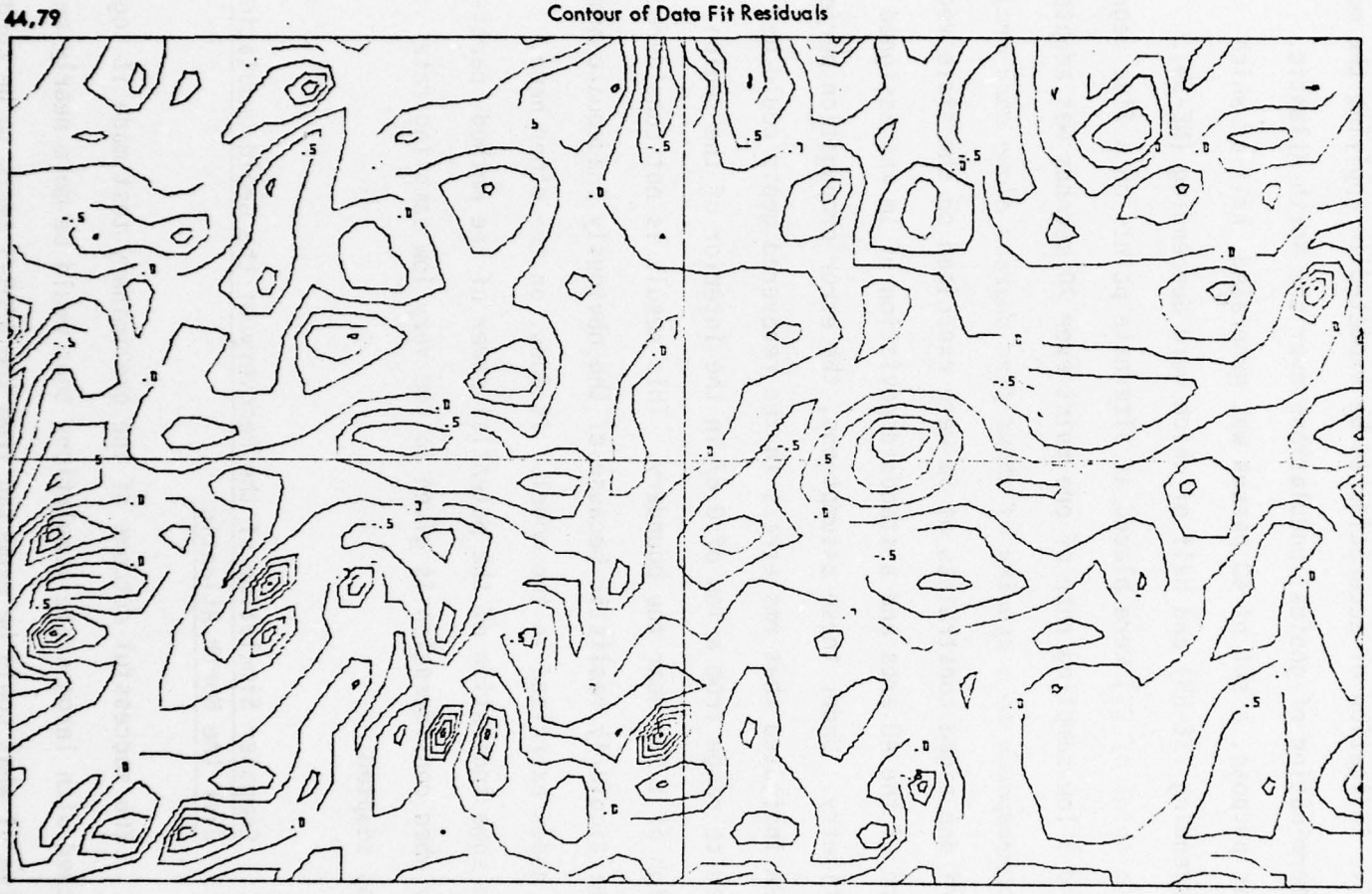

FIGURE 4. Contour Interval = .5 meters
RMS Residual = .75 meters

tentative indication of accuracies to be expected in applying the model to the determination of geoidal undulations over the North Atlantic. For this purpose, a set of 40 passes was generated, half of which were ascending (SE-NW) and half of which were descending (NE-SW). Nodes (*a total of 71*) were placed at alternate points on a five degree grid and a low sampling rate of one point ever 70 seconds was adopted (*this corresponds to a spacing of about five degrees along each arc*). A priori one sigma constraints of 5m were exercised on the state vectors for each of the 40 arcs and a standard deviation of 1m was assigned to the altimetry. Under these assumptions, the error propagation performed by SARRA indicated that rms errors in the recovered geoid could be expected to range from a low of 0.67 in the interior of the region, to a high of 1.93m near the boundary. This result is not considered to be particularly realistic because of the obviously inadequate number of nodes exercised in the model. It does, on the other hand, provide some indication of the potential power of the method, particularly when consideration is given to the very low sampling rate that was adopted.

3.2 Computer Simulation of the Recovery of the Geoid Undulation Over the North Atlantic

The successful outcome of the preliminary test made it logical to proceed with large scale simulations that would be more nearly representative of what could be expected from the GEOS-3 tests to be conducted

over the North Atlantic. For this purpose, the revised version of SARRA was converted to run on the CDC-6600 computer at AFGL. The simulations performed, consisted of two runs based on sets of 320 passes. In all simulations, the nodes were spaced at regular five degree intervals, the total number being 126. In the case of the 200-pass reductions, the altimeter observations were assumed to be spaced at nominal one degree intervals along each arc (*this corresponds to a time interval of 14 seconds*). In the case of the 320-pass reduction, the chosen spacing corresponds to 0.625 degrees, or a time interval of 8.5 seconds. Schematic layouts of the ground tracks for the two sets of simulations are presented in Figures 5 and 6. Other pertinent data concerning the distinguishing assumptions underlying the various simulations are indicated in Table 1.

In Cases 3, 4, 5 and 6, the sigma adopted for altimetry, namely 0.37m, is representative of what would be expected from a data compaction process based on the following considerations:

(a) *an original sampling rate of two per second,*

(b) *an original sigma of 1.0m,* and

(c) *use of a third order midpoint, cubic polynomial filter employing 17 points.*

In Cases 1 and 2, no data compaction scheme was considered to have been exercised; accordingly, here the expected sigma of the raw altimeter observations was exercised at the aforementioned data rate of one point every 14 seconds.

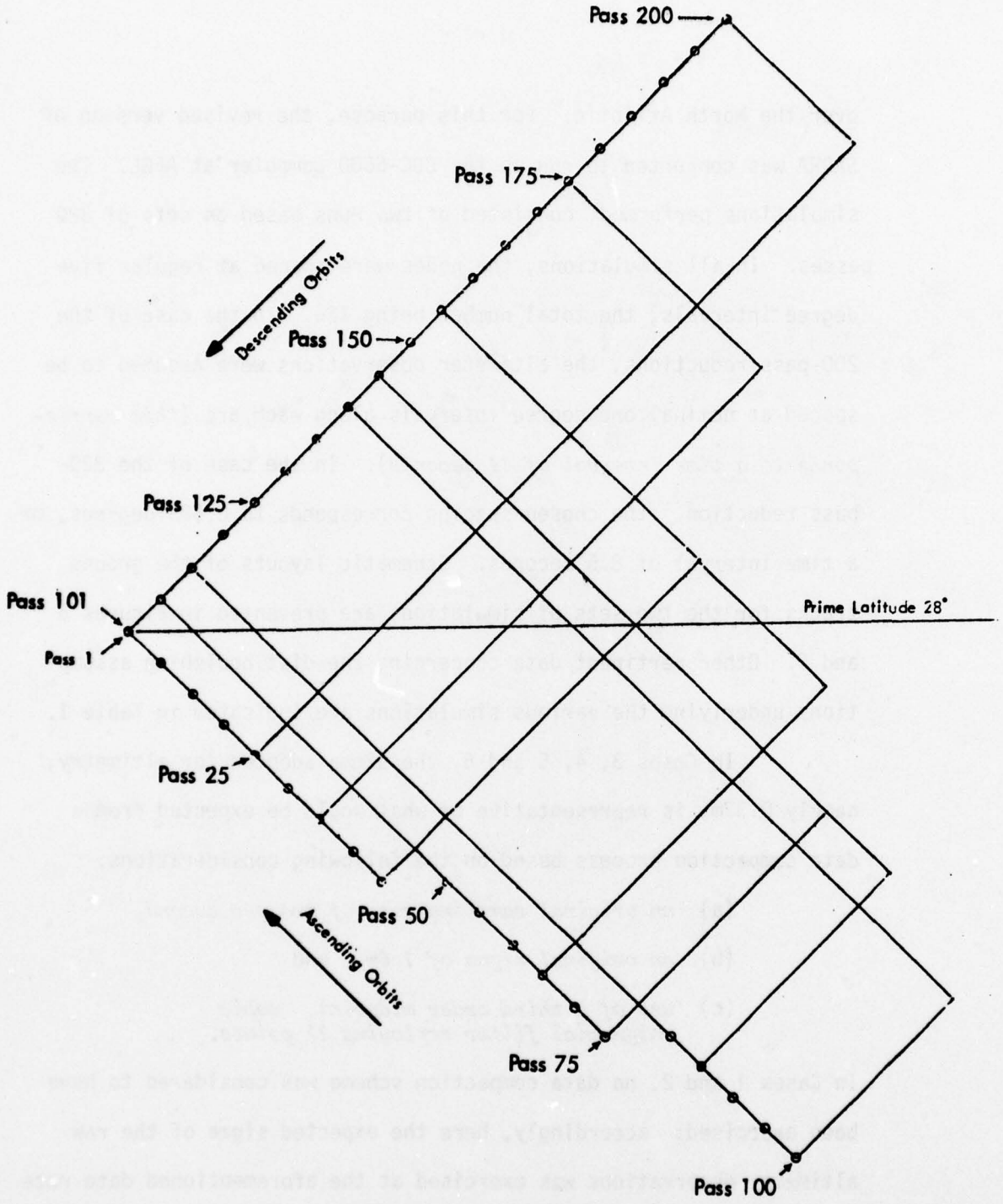

FIGURE 5. Illustration of the Simulation of 200 Satellite Passes That Are Approximately Over the North Atlantic Oceanic Region.

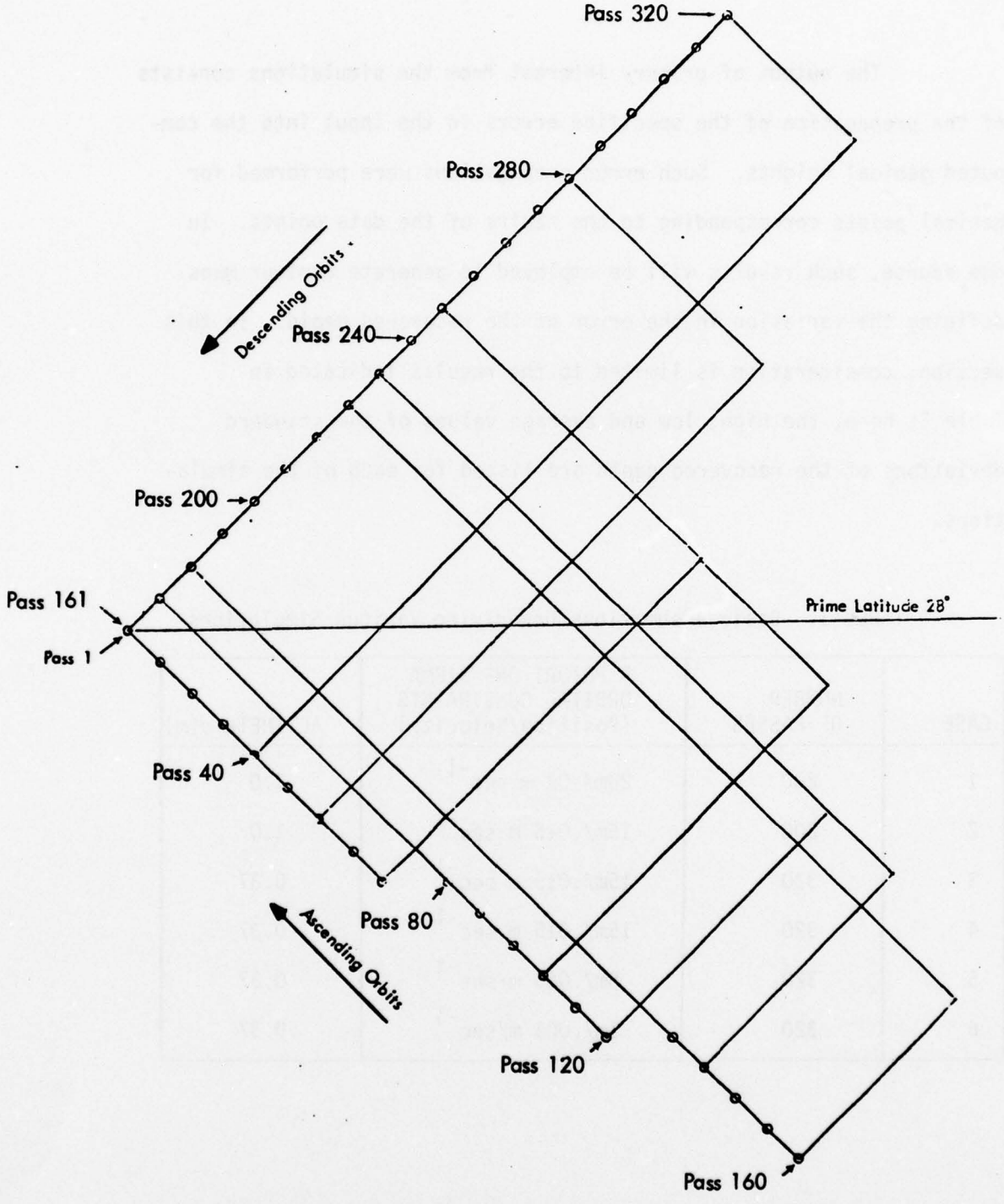

FIGURE 6. Illustration of the Simulation of 320 Satellite Passes That Are Approximately Over the North Atlantic Oceanic Region.

The output of primary interest from the simulations consists of the propagation of the specified errors in the input into the computed geoidal heights. Such error propagations were performed for geoidal points corresponding to the nadirs of the data points. In due course, such results will be employed to generate contour maps defining the variation in the error of the recovered geoid. In this section, consideration is limited to the results indicated in Table 2; here, the high, low and average values of the standard deviations of the recovered geoid are listed for each of the simulations.

TABLE 1. Basic Assumptions Underlying Various Simulations

CASE	NUMBER OF PASSES	A PRIORI ONE SIGMA ORBITAL CONSTRAINTS (Position/Velocity)	ALTIMETRYσ(m)
1	200	20m/.02 m sec^{-1}	1.0
2	200	15m/.015 m sec^{-1}	1.0
3	320	15m/.015 m sec^{-1}	0.37
4	320	15m/.015 m sec^{-1}	0.37
5	320	5m/.005 m/sec^{-1}	0.37
6	320	1m/.001 m/sec^{-1}	0.37

Table 2. Key Results of Simulations

Case	Number of Passes	One Sigma Orbital Constraints (Position/Velocity)	Sigmas of Recovered Geoid		
			High	Low	Average
1	200	20m/.02 m sec^{-1}	1.52	1.34	1.42
2	200	15m/.015 m sec^{-1}	.96	.82	.89
3	320	20m/.02 m sec^{-1}	1.03	.97	1.00
4	320	15m/.015 m sec^{-1}	.54	.46	.51
5	320	5m/.005 m sec^{-1}	.33	.22	.27
6	320	1m/.001m sec^{-1}	.13	.06	.09

The results indicate that general accuracies comfortably better than 1m (*rms*) are to be expected from the reduction of 320 passes, subject to a priori orbital constraints on the order of 15m (Case 4). Because orbital accuracies of considerably better than 5m are a reasonable expectation for the precise reference orbits ultimately to be generated, the results from Cases 5 and 6 suggest that geoidal accuracies on the order of a few tenths of a meter are potentially attainable through the application of the *Short Arc Method*. Attainment of such accuracies in practice will, of course, entail the appropriate application of nodal densification. This, in turn, will require processing of additional passes to maintain a specified level of accuracy. A reasonably conservative extrapolation, in our view, is that with the exercise of some 50 to 75 well-placed, additional

nodes (*raising the total from 175 to 200*) and with the incorporation of perhaps an extra 100 passes (*for a total of over 400*), one can expect SARRA to produce geoidal accuracies generally better than 0.5m when precise reference orbits are employed in the adjustment with one sigma a priori constraints of 5m (*or better*).

3.3 Reduction of the First Available Satellite Altimetry Data from Skylab

The first satellite altimetric data for experimental processing with the SARRA computer program became available from altimetric observations made by Skylab (*SL-2*). Two passes were processed through the SARRA computer program for the purpose of testing the basic data flow procedures and to evaluate the adequacy of the program in reducing the data. Figure 7 shows the ground track of the two passes plotted by the DBA CALCOMP plotter. Pass 9 begins off the east coast of the United States and extends approximately 15 to 20 degrees below the equator. Pass 4 begins off the east coast and extends over Puerto Rico.

Mid-arc state vectors were computed from ephemeris data provided by NASA for initial orbital estimates of each arc. Data editing procedures were designed and performed on the observation data prior to SARRA processing. These included, primarily, an automatic rejection of gross error indicated by the residual altimetry parameter in the SL-2 EREP format and a three-sigma criterion edit after a ninth order polynomial data fit.

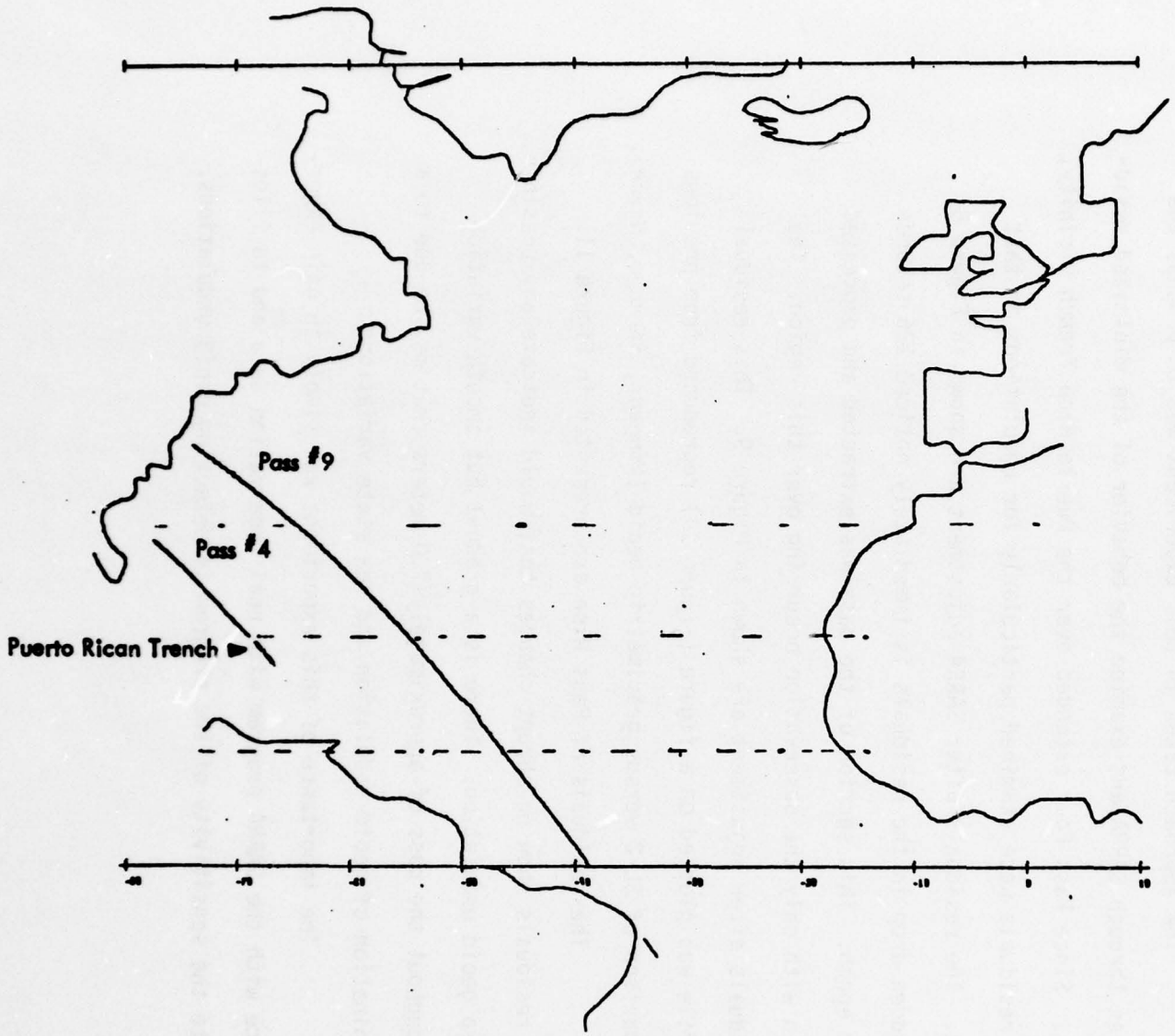

FIGURE 7. Skylab Ground Tracks

The approach taken in this experiment was to process the passes through SARRA and examine the behavior of the minimized residuals. Since Pass Four extended over the Puerto Rico Trench vicinity, the residuals were examined particularly for undulations in that area. The residuals after SARRA adjustment are shown in Figure 8. A sudden drop in the residuals is immediately noticed 126 seconds from epoch. This section of the pass was extracted and processed again with only the observation occurring over this region. The residuals after adjustment are shown in Figure 9. This residual profile was plotted on a figure (*Figure 10*) reproduced from previous comparison of SL-2 versus gravimetric geoid (*Vincent, Strange, Marsh*).

The residuals of Pass Nine are presented in Figure 11. The residuals show no abrupt changes that would indicate any possible sharp geoid undulation. There is a gradual but smooth variation throughout the pass of approximately 7.0 meters that may be due to a combination of geoid undulation and sea state variations.

The importance of this experiment was simply to gain experience with the SARRA program with real observation data and to illustrate the sensitivity of the program in detecting geoid undulations.

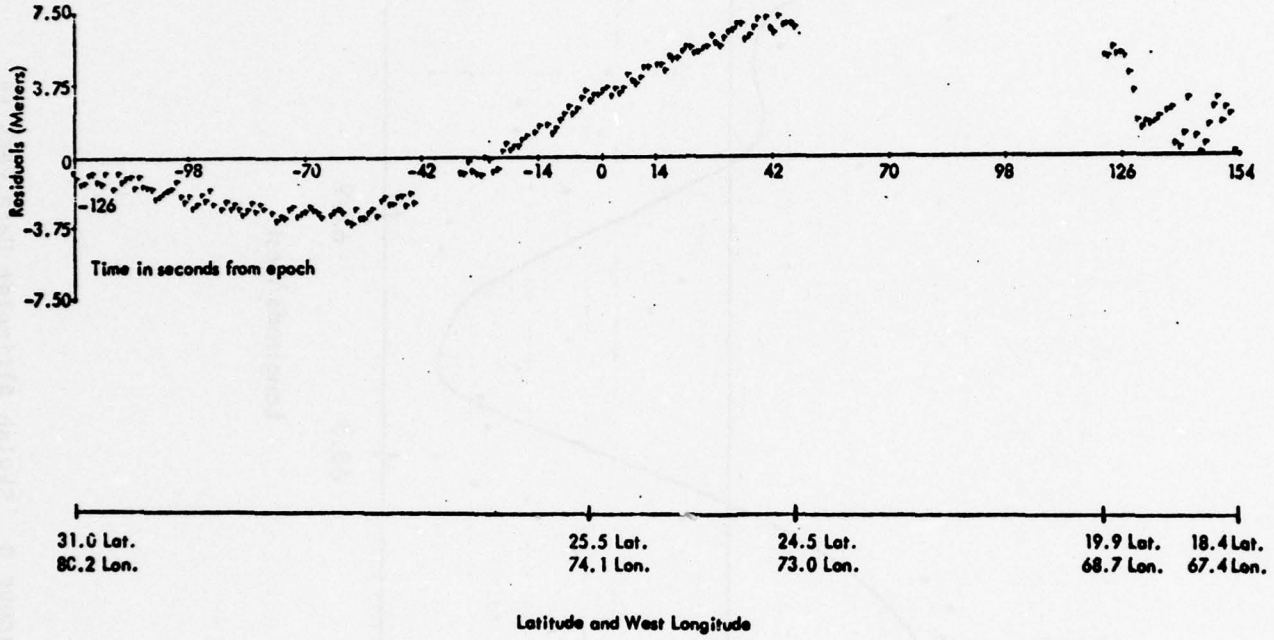

FIGURE 8. Skylab Altimeter Data Pass #4

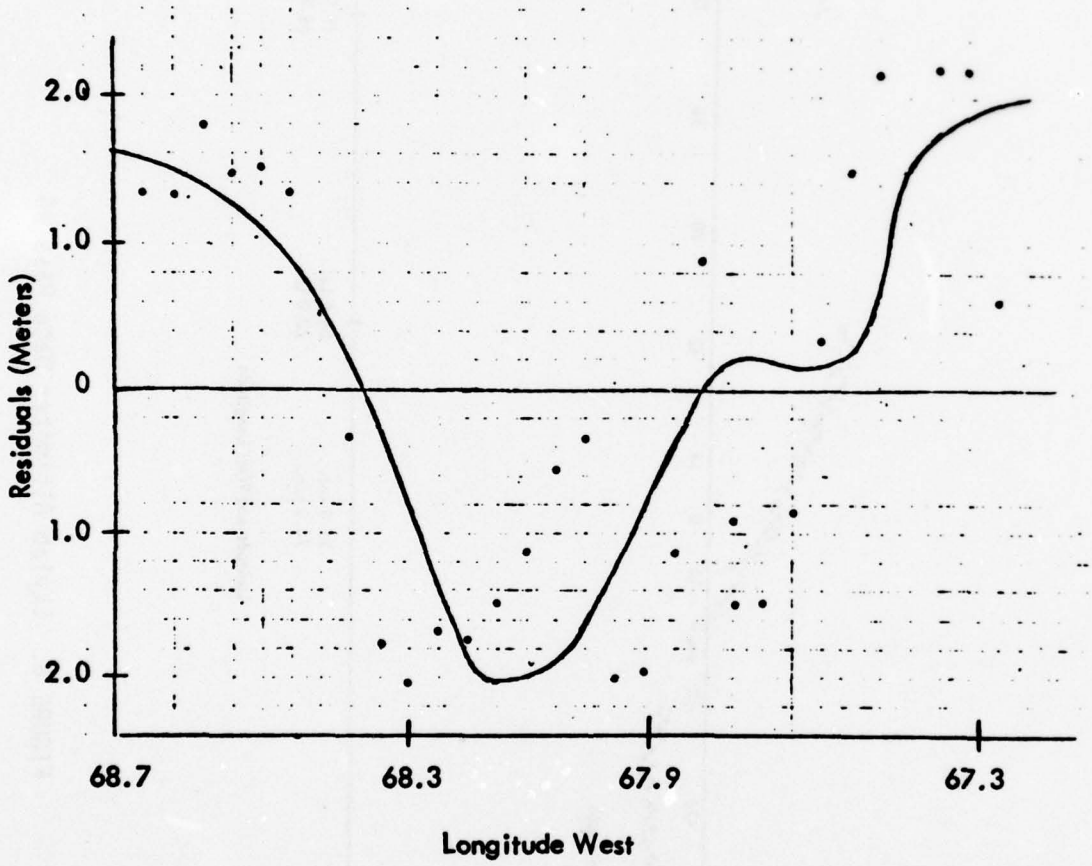

FIGURE 9. Skylab Altimeter Data Pass #4
Puerto Rico Trench Only

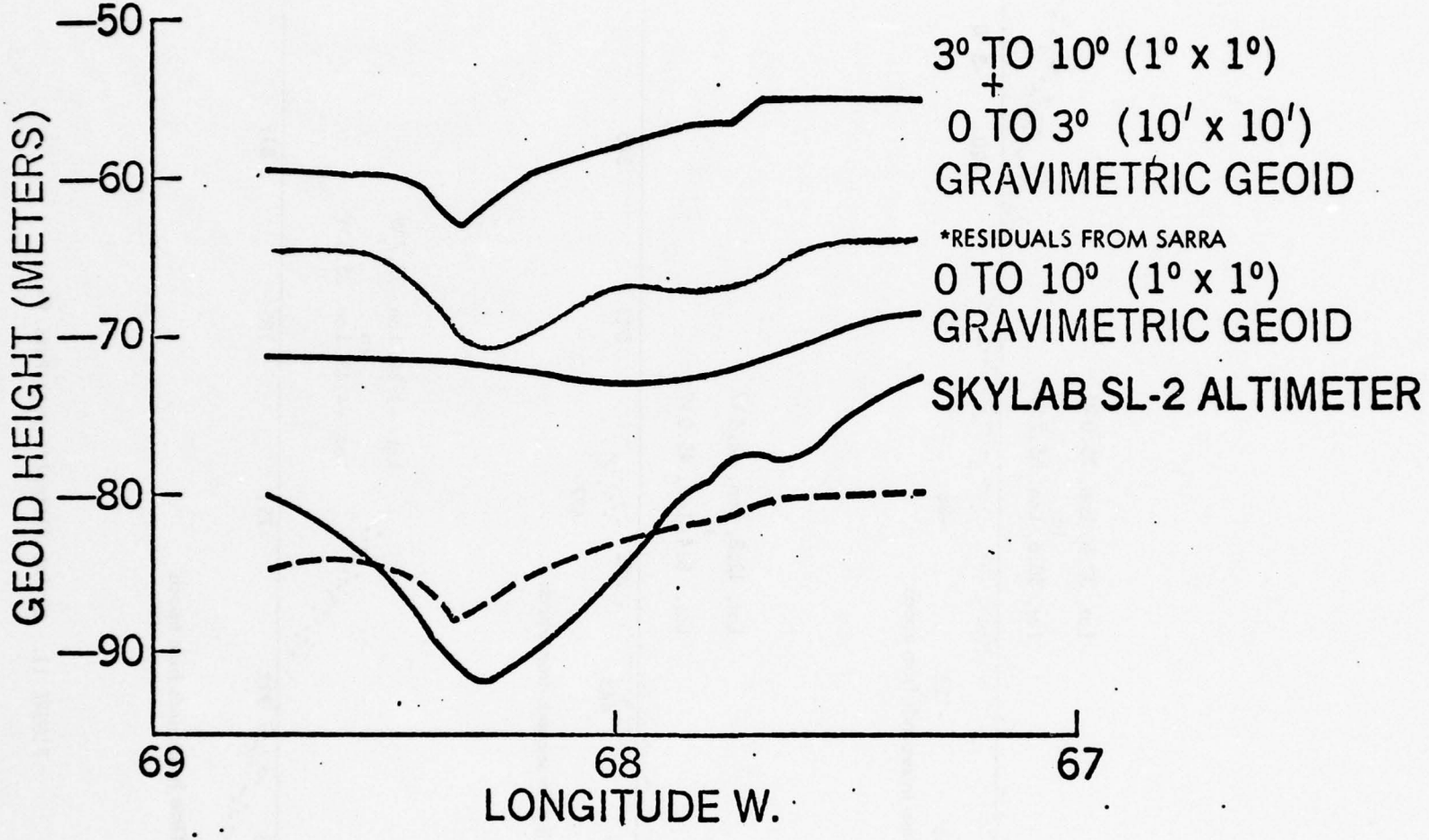

Result from DBA SKYLAB SL-2 altimeter data plotted on a reproduction of Figure 7 from Marsh, Vincent "DETAILED GRAVIMETRIC GEOID FOR THE GEOS-C ALTIMETER CALIBRATION AREA".

FIGURE 10. Comparison of Gravimetric Geoid with Skylab Altimeter Data

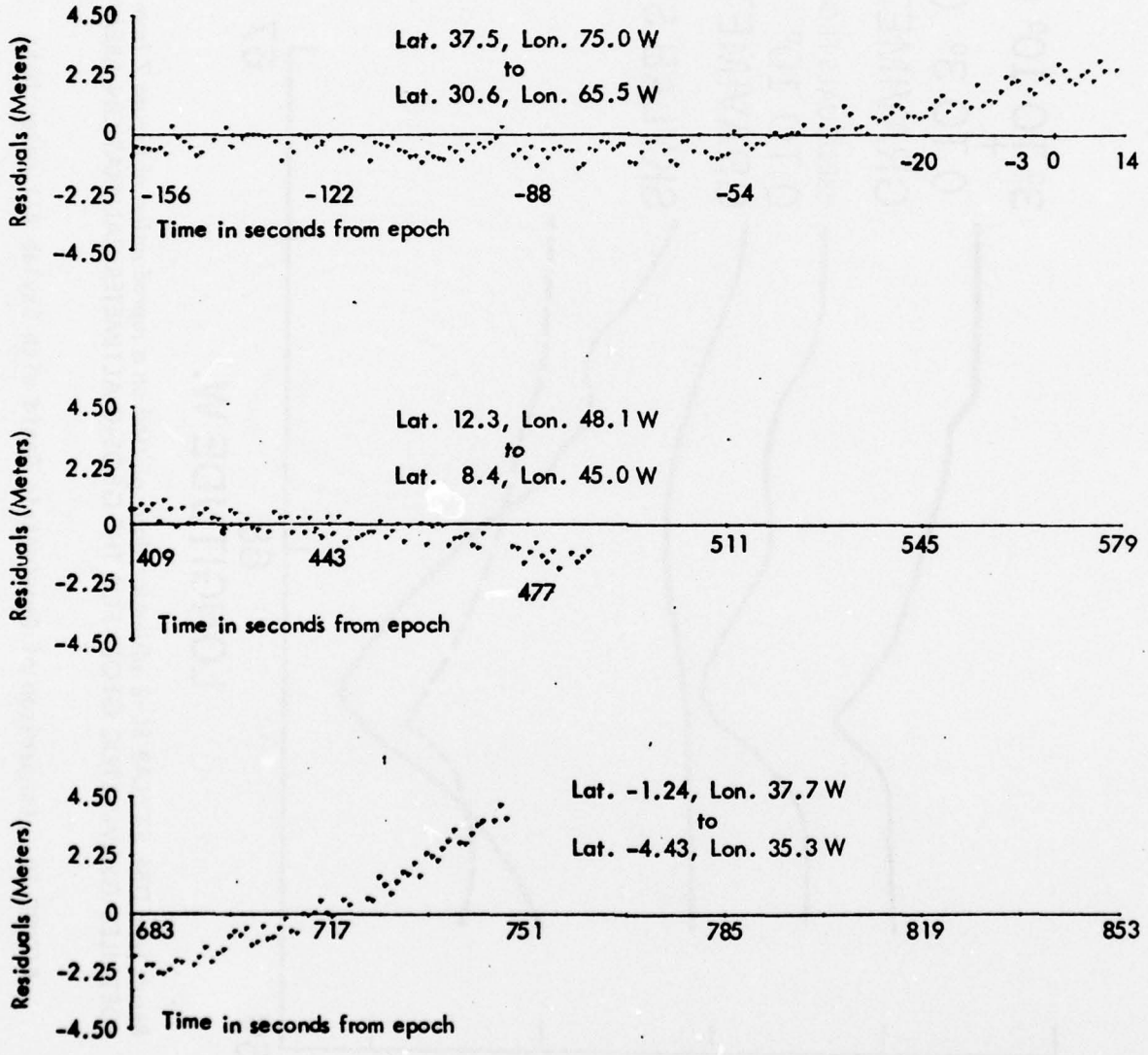

FIGURE 11. Skylab Altimeter Data Pass #9

3.4 Preliminary Reduction of GEOS-3 Altimetry Data Over the North Atlantic Ocean

Some preliminary reductions were performed with GEOS-3 altimetric observations concentrated over the western portion of the North Atlantic Ocean. The observational data was provided to AFGL by NASA and consisted of 112 passes (*Figure 12*). These data sets provided an opportunity to test the basic mathematical models used to represent the geoid surface. The results of these reductions were presented at the American Geophysical Union (*AGU*) fall meeting held in December 1976 at San Francisco.

The distribution of this data set was not adequate for a geoid undulation determination of the entire North Atlantic and was not suitably located for the detailed examination of such fine features as the Puerto Rico Trench. However, it did provide adequate data to evaluate the performance of SARRA computer program in an operational environment and demonstrate the potential accuracy of the approach.

The short arc approach to these reductions may be visualized along the following lines:

(a) *reference orbits accurate to approximately 20 meters may be obtained from routine global tracking;*

(b) *the reference orbits are divided into subarcs, situated over oceanic regions and are limited in length to no more than a quarter revolution;*

(c) *each sub-arc is treated as an independent orbit with the epoch at mid-arc having a state vector subject to a priori constraints consistent with the estimated accuracy of the reference orbits;*

(d) *observational equations are formed from satellite altimetric measurements for each sub-arc for the mathematical model chosen to represent the oceanic geoid;*

(e) *the adjustment simultaneously recovers the coefficients of the geoid surface model and revised estimates of the state vectors for all sub-arcs (which are unlimited in number).*

3.4.1 Unknowns and Constraints Used in the Reductions. The SARRA program is designed to determine surface coefficients as designated by nodal points that lie within the boundaries of a dense selection of height measurements. In addition to determining the coefficients of each nodal point, the program solves the six orbital parameters for each arc.

The orbit parameters were assumed subject to a priori constraints of 20.0 meters in position and .005 m/sec in velocity. The a priori standard error was assumed to be 1.0 meter for all altimetric measurements.

During the initial preprocessing of the GEOS-3 data, certain characteristics were identified for editing criteria. The first editing level automatically examined altimetry measurements for gross errors that occurred from data handling procedures, such as tape parity errors and measurement identification problems. The

second editing procedure was to examine the altimeter measurements for continuity and to eliminate abrupt point to point changes. The final editing is based on a three-sigma criteria when compared to a polynomial smoothing function.

3.4.2 Results. The reduction of GEOS-3 altimetric measurements over the North Atlantic included data from 112 passes. The surface grid formed by these passes was dense in the western portion, and very sparse in the northern. It did not extend to the southeastern portion of the North Atlantic. Figure 22 illustrates the surface geometry of the GEOS-3 ground tracks. The figure also reflects the nodal selection used for this reduction. Due to the variations in data densities from one area to the other, a proper value for k (*Equation 1, Section 3.2*) had to be determined for representing the entire North Atlantic grid. It was found to be important that the choice of $\delta = ka$ bear a balanced relationship to the typical spacing of the nodes. The more closely spaced the nodes, the smaller the logical choice for δ. This allows the surface in the vicinity of any given data point to be determined predominantly by those kernel functions of nearby nodes and yet prevents any one node from exerting total dominance.

Figure 13 shows contours of the derived geoid undulations using the multiquadric function approach. In general, the entire geoid agrees favorably with the *Marsh* and *Chang* gravimetric geoid, especially in the western portion of the area where the data density

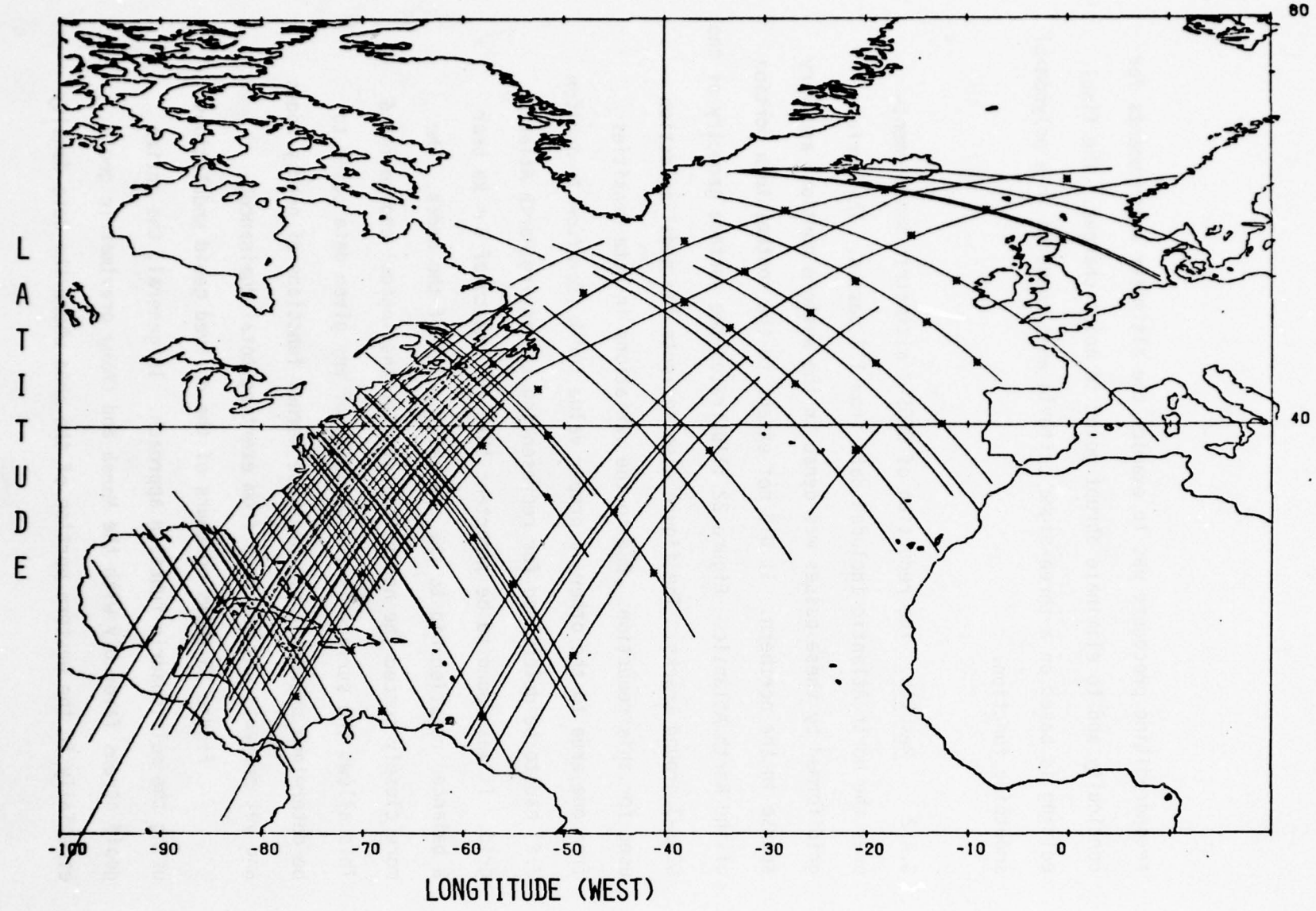

FIGURE 12. Calibration Area GEOS-3 Ground Tracks

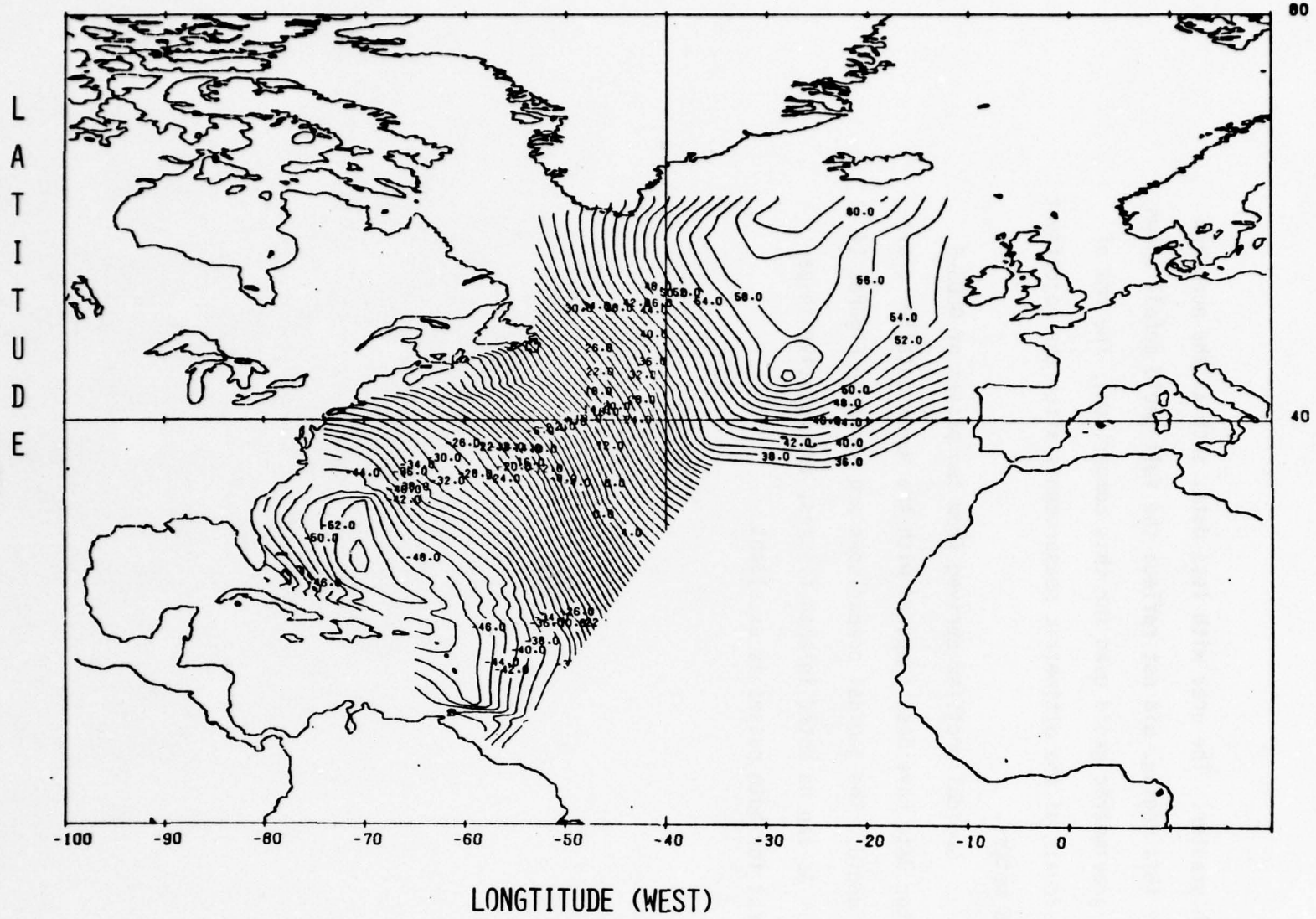

FIGURE 13. Geoid Contour Map of the GEOS-3 Calibration Area

is much greater. The area with less data, such as the northern part of this region, did not reflect the full geoid detail shown by the gravimetric geoid used for this comparison. The rms of the residuals of the altimetric measurements after the adjustment was 1.8 meters.

Geoidal profiles derived from two passes of GEOS-3 altimeter data have been compared with the *Marsh* detailed gravimetric geoid. The geoidal comparisons are shown in Figures 14 and 15. As can be noted in both figures, the relative shape agreement for both passes is excellent.

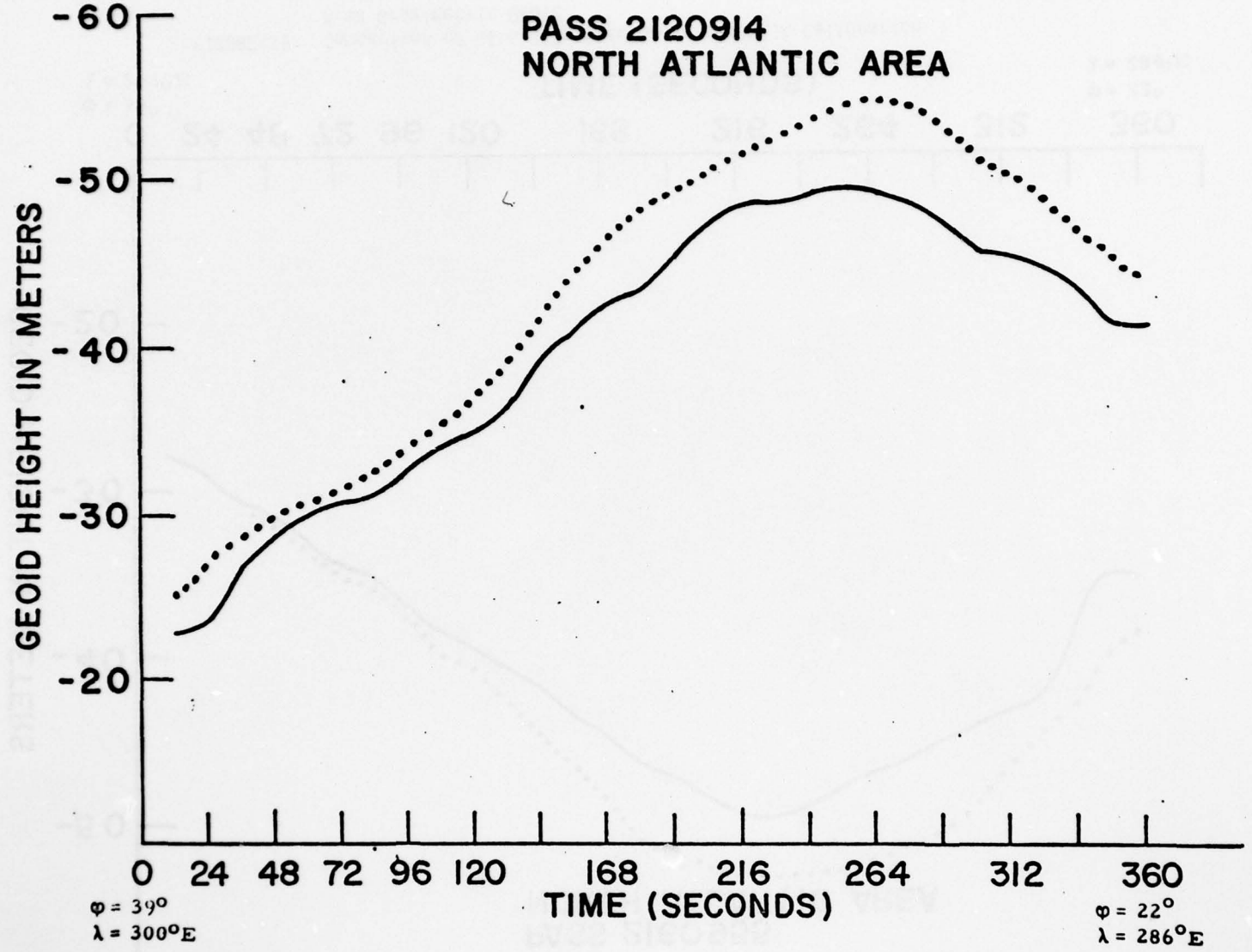

FIGURE 14. Comparison of Geos-3 derived Geoid and NASA Calibration Area Gravimetric Geoid

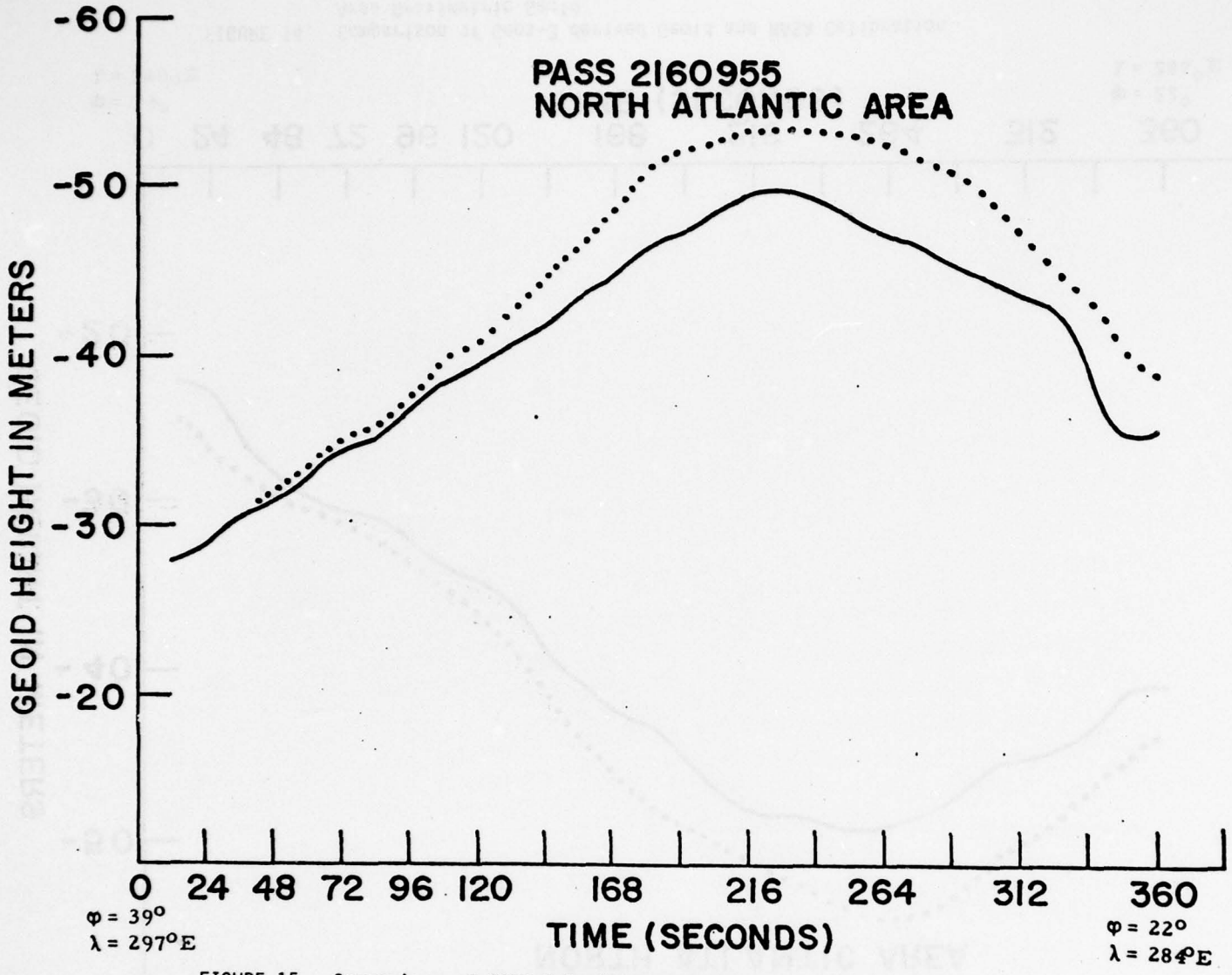

FIGURE 15. Comparison of GEOS-3 Derived Geoid and NASA Calibration Area Gravimetric Geoid

SECTION 4

MATHEMATICAL SURFACE MODELS

As stated earlier, the model originally used in SARRA for representing the oceanic geoid, was a derivation of the spheroidal multiquadric analysis developed by *Hardy* (*1972*). This model provides convenient flexibility when processing data collected over extremely small surface areas with a dense set of measurement data. It is independent of spherical harmonic representation of the geoid, thereby, eliminating the requirement to solve for high order and degree spherical harmonic coefficients. However, in the course of preliminary data processing of GEOS-3 altimetric data, it became evident that the observation data was very sparse in certain areas of the North Atlantic Ocean. Therefore, another model, namely the covariance function by *Heiskanen* and *Moritz* was investigated and implemented into the SARRA computer program to provide more flexibility when processing sparse sets of data.

4.1 The Covariance Function

The detail derivation of the covariance function as applied in the SARRA computer program may be found in Appendix A of this report. The expression for the partial derivative matrix is defined here for the formation of normal equation.

The covariance function $D(\psi)$ for geoid undulations is obtained by averaging the product $N\,N^1$ over the unit sphere,

$$D(\psi) = M\{NN^1\}; \tag{1}$$

N and N^1 in this expression are the geoid undulations at any two points separated by the symbol M indicating the average over the unit sphere, namely

$$M\{\cdot\} \equiv \frac{1}{4\pi} \iint_{\sigma} (\cdot)\, d\sigma,$$

where σ represents the surface of this sphere and $d\sigma$ is the element of surface area. The covariance function may be expressed as (*Heiskanen and Moritz, 1967*):

$$D(\psi) = \sum_{n=2}^{\infty} d_n \; P_n \; (\cos \psi), \tag{2}$$

Where

$$d_n = \frac{R^2}{G^2(n-1)^2} \sum_{n=o}^{n} (\Delta c_{nm}^{-2} \;\; \Delta s_{nm}^{-2}) \tag{3}$$

the quantities d_n are called "degree variances" for geoid undulation and $\Delta\bar{s}_{nm}$ are the corrections to the a priori coefficients of the spherical harmonic expansion of the geopotential. The parameter R is the mean radius of the earth and G is the mean gravity of the earth's surface. By $\psi = 0$, we have from (2) by substitution

$$D(0) = \sum_{n=2}^{\infty} d_n \tag{2^1}$$

The weighted sum of covariance functions between point P_i and a number of selected nodal points P_j gives the undulation N_i at P_i:

$$N_i = \sum_j c_i D(\psi_{ij}), \tag{4}$$

where c_j are the weights which must be determined and ψ_{ij} is the spherical distance between P_i and P_j.

4.2 The Spheriodal Multiquadric Model

The expression for the geoidal model expressed in terms of the spheroidal multiquadric functions is the same equation (4) above. The only difference is the replacement of the covariance function $D(\psi_{ij})$ with the "kernal function" of the form

$$\psi_{ij} = \frac{r_j^2}{a\left[\left(|X_g - X_j| + ka\right)^2 + \left(|Y_g - Y_j| + ka\right)^2 + \left(|Z_g - Z_j| + ka\right)^2\right]^{\frac{1}{2}}} \tag{1}$$

Where

$$X_{gi} = X_{si} - H_i \cos \phi_i \cos \lambda_i$$
$$Y_{gi} = Y_{si} - H_i \cos \phi_i \sin \lambda_i$$
$$Z_{gi} = Z_{si} - H_i \sin \phi_i$$

And

H_i = Altimetry measurement of the geoid point

r_i = Geocentric radius to the geoidal point X_{gi}, Y_{gi}, Z_{gi}

ka = An arbitrary fraction of the semi-major axis a

X_j, Y_j, Z_j = arbitrarily specified nodes.

X_{si}, Y_{si}, Z_{si} = geocentric coordinates of the ith sub-satellite point

SECTION 5

FORMATION AND SOLUTION OF THE NORMAL EQUATIONS

The observation equation for a single pass is taken from equation (13) of Appendix A and written as follows:

$$V_i = \left\{ -\left[D(\psi_{i1}) \ , \ldots , \ D(\psi_{ij}) , \ldots \right] \Big\vert \quad \frac{\delta(R_i - r_i')}{\delta(X, \ldots \dot{Z})_0} \right\} X$$

$$X \quad \left[\begin{array}{c} dc_1 \\ \vdots \\ dc_j \\ \vdots \\ \hline dx \\ \vdots \\ dz \end{array} \right] \quad + \ (R_i^0 - r_i' - H_i + d_i \ ). \qquad (1)$$

where

V_i = residual

R_i^0 = initial estimate of the radial distance to the sub-satellite point

d_i = small quantity to correct for non-geocentric direction of the altimetry measurement

dc_i = coefficient matrix of nodes

dx,...dz = coefficient matrix of orbit parameters

Here the subscripts i and j refer to the i^{th} sub-satellite point and the j^{th} node of a single pass. Later the subscript k will be introduced to refer to the k^{th} arc. The "kernal function", $D(\psi_{ij})$, is selected by input to be either the covariance function or the multiquadric function to represent the geoid surface as described above (*Section 4.1, 4.2*).

Equation (1) is written in terms of the matrix of partial derivatives for the i^{th} altimetry measurement point in the form.

$$B_i = \frac{1}{\sigma_h} \left[\dot{B}_i \qquad \ddot{B}_i \right] \tag{2}$$

Where

σ_h = standard error of the altimeter measurement

$\dot{B}_i$ taken from equation (1) as

$$\dot{B}_i = - \left[D(\psi_{i_1}) \quad D(\psi_{i_2}) \ldots D(\psi_{ij}) \ldots . D(\psi_{in}) \right], \tag{3}$$

Where

n = number of nodal points

$$\ddot{B}_i = \frac{\partial(R_i - r_i)}{\partial(X, \ldots \dot{Z})_0} \quad . \tag{4}$$

The partials with respect to the orbital parameters have been refined by *Blaha (1976)* which introduced a faster convergence in the adjustment and in most cases removed the need for iterating the solution. The detailed description of the parameters in (4) may be found in Appendix A.

The discrepancy term is defined by:

$$E_i = R_i - r_i - H_i + d_i \; . \tag{5}$$

The normal equations for the K^{th} arc are written as:

$$N_k \delta_k = c_k \tag{6}$$

where

$$N_k = \sum_{i=1}^{m} B_i^T B_i$$

$$c_k = \sum_{i=1}^{m} B_i^T \varepsilon_i$$

δ_k = correction vector

and

m = number of altimeter measurements in the k^{th} arc.

The normal equations generated by this arc may be written in the matrix form

$$\begin{bmatrix} \dot{N}_k & \overline{N}_k \\ \overline{N}_k & \ddot{N}_k \end{bmatrix} \quad \begin{bmatrix} \dot{\delta}_k \\ \ddot{\delta}_k \end{bmatrix} = \begin{bmatrix} \dot{c}_k \\ \ddot{c}_k \end{bmatrix} \; . \tag{7}$$

Introducing a priori orbital constraints for the k^{th} arc leads to the following system of normal equations.

$$\begin{bmatrix} \dot{N}_k & \bar{N}_k \\ \bar{N}_k^T & \ddot{N}_k + \ddot{\omega}_k \end{bmatrix} \begin{bmatrix} \dot{\delta}_k \\ \ddot{\delta}_k \end{bmatrix} = \begin{bmatrix} \dot{c}_k \\ (\ddot{c}_k - \ddot{\omega}\ \ddot{\xi})_k \end{bmatrix} \tag{8}$$

Where

$\ddot{\omega}_k$ = the inverse of the covariance matrix of the a priori values of the state vector.

$\ddot{\xi}_k$ = the difference between the a priori values of the state vector and the values currently being employed as current approximations. Initially, $\ddot{\xi}$ may be considered zero for the first iteration.

The expansion of equation (8) is now introduced for the simultaneous reductions of all adjustable parameters for all arcs.

$$\left[\begin{array}{c|cccc} \dot{N} & \bar{N}_1 & \bar{N}_2 & \cdots & \bar{N}_S \\ \hline N_1^T & (\ddot{N} + \ddot{\omega})_1 & & & \\ N_2^T & & (\ddot{N} + \ddot{\omega})_2 & & \\ \vdots & & & \ddots & \\ \bar{N}_S^T & & & & (\ddot{N} + \ddot{\omega})_S \end{array}\right] \left[\begin{array}{c} \dot{\delta} \\ \hline \dot{\delta}_1 \\ \dot{\delta}_2 \\ \vdots \\ \dot{\delta}_S \end{array}\right] = \left[\begin{array}{c} \dot{c} \\ \hline (\ddot{c} - \ddot{\omega}\ \ddot{\xi})_1 \\ (\ddot{c} - \ddot{\omega}\ \ddot{\xi})_2 \\ \vdots \\ (\ddot{c} - \ddot{\omega}\ \ddot{\xi})_S \end{array}\right] \tag{9}$$

in which

$$\dot{N} = \sum_{k=1}^{s} N_k \qquad (10)$$

$$\dot{c} = \sum_{k=1}^{s} \dot{c}_k$$

The solution of the normal equations (9) involves n unknowns (*one for each node*) plus six for each arc. The number of arcs, s, in a solution may grow to several thousand, thereby, creating a large system with rank, r = n + 6s. The solution to this large system of normal equations is made practical by virtue of exploiting the patterned characteristics. Full details of derivation may be found in *Brown (1958)* or in *Brown, Trotter (1969)*. The computational steps follow.

Compute the auxiliaries for the k^{th} pass

$$\underset{(6,n)}{Q_k} = \underset{(6,6)}{(N + \bar{w}^{-1})_k} \; \underset{(6,n)}{N_k^T} \qquad (11)$$

$$\underset{(n,n)}{R_k} = \underset{(n,6)}{\bar{N}_k} \; \underset{(6,n)}{Q_k} \qquad (12)$$

$$\underset{(n,n)}{S_k} = \underset{(n,n)}{\dot{N}_k} \; \underset{(n,n)}{R_k} \qquad (13)$$

$$\underset{(n,1)}{\bar{c}_k} = \underset{(n,1)}{\dot{c}} - \underset{(n,6)}{Q} \; (\underset{(6,1)}{\ddot{c}_k} - \underset{(6,6)}{\ddot{w}_k} \; \underset{(6,1)}{\ddot{\xi}_k}) \qquad (14)$$

As the S_k and $\bar{c}_k$ matrices are formed for each pass, they are summed into the matrices S and $\bar{c}$ by

$$S = \sum_{k=1}^{s} S_k \tag{15}$$

and

$$\bar{c} = \sum_{k=1}^{s} \bar{c}_k \quad . \tag{16}$$

The solution for the geoidal coefficients is computed by

$$\dot{\delta} = S^{-1} \bar{c} \qquad (n,1)(n,n)(n,1) \tag{17}$$

The solution $\ddot{\delta}_k$ for the adjusted corrections to the state vector for the k^{th} arc is computed by

$$\ddot{\delta}_k = (\ddot{N}_k + \ddot{\omega}_k)^{-1} \quad (\ddot{c}_k - \ddot{\omega}_k \ddot{s}_k) - Q_k \dot{\delta}_k. \tag{18}$$

The error propagation for a given geoid point may be computed by

$$\sigma_{ii} = \sigma_{ii} \quad (\dot{B}_{ij} S^{-1} \dot{B}_{ij}^T)^{\frac{1}{2}} \tag{19}$$

where the B_p partial derivative matrix is computed for the corresponding ϕ, λ as in equation (3).

SECTION 6

ANALYSIS OF RESIDUALS

Careful pass-by pass examination of the plotted altimeter residuals can be made in order to uncover any localized systematic effects signifying insufficiently modelled geoid undulations. This is especially important to areas corresponding to known bathymetric and surface features such as the Puerto Rico Trench, the Mid-Atlantic Ridge, sea mounts, etc. Where indicated from analysis of residuals, additional nodes can be introduced at appropriate locales. The process of nodal densification for more detailed local definition of the geoid will exercise supplementary observations from any additional passes that may be available over that area.

Altimeter residuals will reflect not only unmodelled geoid undulations, as just discussed, but also various quasi-systematic trends attributable to ocean dynamics such as tides, wind stress, swells, currents, etc. With the exception of currents, such phenomena are ephemeral or cyclic and thus, random over a sufficiently large number of passes. Except near shore lines, their amplitudes are generally less than one meter and will have only a slight influence on the geoid recovery. Although the residuals obtained following nodal densification contain a wealth of information, it is beyond the scope of this contract to subject the residuals to such a detailed analysis.

This section will present the procedures that may be pursued in facilitating the ultimate residual analysis. As thousands of passes have been processed with the computer program SARRA over a course of months or even years, a very stable data base of normal equations and coefficients of the geoid surface will be established. As new observation data is collected (*especially in regard to SEASAT A*), one only has to form the normals of the new passes and sum them into the accumulated normals saved in the data base in order to update the solution.

Once the geoid coefficients become sufficiently stable (*meaning additional measurement makes insignificant changes to the geoid*), we may treat the geoid coefficients as being perfectly known and process individual passes for detail residual analysis. The only adjustable parameters are the six state vector parameters (X, Y, Z, $\dot{X}$, $\dot{Y}$, $\dot{Z}$). This leads to a simple adjustment that could be processed on a mini-computer or a hardwired microprocessor requiring less than 1000 words of memory. It could even be envisioned as a real time monitoring processor with the appropriate communication and transmission interface.

The solution of the single pass may be accomplished as follows:

the observation equation is written as

$$r_i = \frac{d\,(R - r')_i}{d\,(X, Y, Z, \dot{X}, \dot{Y}, \dot{Z})} \begin{bmatrix} d\,X \\ d\,Y \\ d\,Z \\ d\,\dot{X} \\ d\,\dot{Y} \\ d\,\dot{Z} \end{bmatrix} + \left[R - r' + d - H\right]_i \tag{1}$$

where all parameters are identical to those described in Section 4. The matrix of partial derivations of the i^{th} altimeter measurement is

$$\dot{\dot{B}}_i = \frac{d\,(R - r')}{d\,(X, Y, Z, \dot{X}, \dot{Y}, \dot{Z})} \tag{2}$$

the discrepancy term

$$E_i = R_i - r'_i + d_i - H_i + r_i \tag{3}$$

The geoid parameter, r_i, is computed from the geoid coefficients, $\dot{\delta}$, equation (18, Section 5) saved from the data base (*previous SARRA reduction*) and partials, B_i, of the geoid parameters for the i^{th} measurement. The B_i matrix is computed and formed by the same process as in Section 4.1, equation (2) or Section 4.2, equation (1), depending on which model was used to represent the geoid surface in the master reduction. The solution for r_i is

$$\underset{(1,1)}{r_i} = \underset{(1,n)}{\dot{B}_i} \quad \underset{(n,1)}{\dot{\delta}} \tag{4}$$

where

n = number of nodes used in the master reduction and the partials, $\dot{B}_i$, are computed for all nodes in the master solution.

The normal equations are written in matrix form as

$$\ddot{N} \quad \ddot{\delta} \quad = \quad \ddot{c} \qquad (5)$$

where

$$\ddot{N} = \sum_{i=1}^{m} \ddot{B}_i^T \ \ddot{B}_i$$

;

$$\ddot{c} = \sum_{i=1}^{m} \ddot{B}_i^T \ E_i$$

$$\ddot{\delta} = \begin{bmatrix} d\,X \\ d\,Y \\ d\,Z \\ d\,\dot{X} \\ d\,\dot{Y} \\ d\,\dot{Z} \end{bmatrix}$$

and

m = number of observations for the arc.

In order to make the above solution determinable for δ, the orbital constraints must be applied as in Section 5.

Equation (5), above, is modified to accommodate orbital constraints in the form

$$(\ddot{N} + \ddot{w}) \ \ddot{\delta} \quad = \ddot{c} - \ddot{w} \ \ddot{\xi} \qquad (6)$$

Since the value for $\ddot{\xi}$ is normally zero unless some correction is known in regard to the state vector, the solution for $\ddot{\delta}$ becomes

$$\underset{(6,1)}{\ddot{\delta}} = \underset{(6,6)}{(\ddot{N} + \ddot{\omega})^{-1}} \quad \underset{(6,1)}{\ddot{c}} \tag{7}$$

By substituting $\ddot{\delta}$ into equation (1), we solve for the residuals, r_i for all points on the arc. These could be output to plot displays on a CRT type monitor.

The above process requires minimal computer core requirements and the largest matrix required is (6,6) for the $\ddot{N}$ and $\ddot{w}$ matrix. The processing time would also be minimal.

SECTION 7

FINAL REDUCTIONS OF THE NORTH ATLANTIC OCEANIC GEOID

The major objective of this effort was to develop the appropriate computer software for reducing altimetric observations and to apply this software in the determination of the North Atlantic oceanic geoid. The initial coverage was expected to be similar to that depicted in Figure 1 and become more densified as more observations were made by GEOS-3. However, the availability of data did not provide the desired coverage over the entire North Atlantic, nor the density in key areas outside the calibration area. This data set provides enough coverage (*see Figure 16*) for an extensive testing of the capabilities of the software system in detecting and modelling detail features.

The final reductions are essentially extensions to the preliminary reductions presented in Section 3.4

7.1 Unknowns and Constraints Used in the Reductions

The same set of nodal points, data and orbital constraints were used for both the spheroidal multiquadric and the covariance function models. The number of nodes used was 47 and the number of

passes was 236. This resulted to a total of 1463 unknowns (*6 x passes + nodes*) that were recovered simultaneously. The constraints exercised for the state vectors in terms of north, east and up were

σ_n = *20.0 meters*

σ_e = *20.0 meters*

σ_u = *20.0 meters*

$\sigma_{\dot{n}}$ = *.010 meters/second*

$\sigma_{\dot{e}}$ = *.010 meters/second*

$\sigma_{\dot{u}}$ = *.010 meters/second.*

These orbital constraints are chosen to be relaxed enough to accommodate expected errors in the generated state vectors. The altimetric observations were treated as subject to 1.0 meter error (*one sigma*) for the adjustments and error propagation.

The selection of nodal positions are illustrated by Figure 16.

7.2 Reduction Results

The reduction of the GEOS-3 altimetric measurements include data from 236 passes of GEOS-3 over the North Atlantic. The surface grid formed by the ground track of these passes was very dense in the western portion and sparse elsewhere. Figure 16 illustrates the surface geometry of the grid.

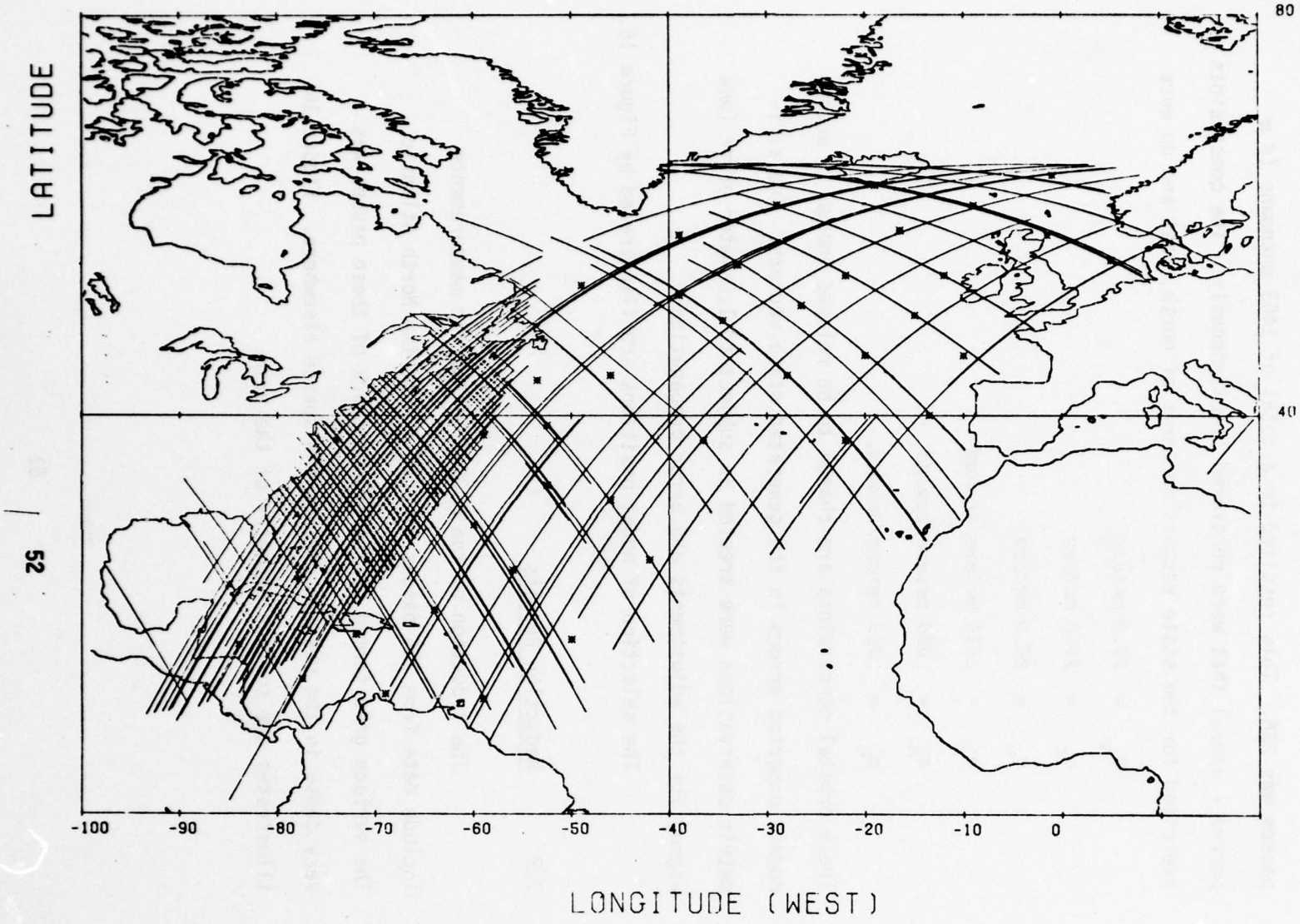

FIGURE 16. Ground Track of Satellite Passes over the North Atlantic Ocean

It has been experienced (*reference* 11) in previous applications of the spheroidal multiquadric model that a proper choice of $\delta = ka$ (*Equation 1, Section 3.2*) is important in keeping a balanced relationship to the typical spacing of the nodes. The constant δ controls the degree of correlation between nodes and as the value of δ decreases, the correlation between nodes decreases (*see reference 1*). The present reductions varied in data density from one portion of the North Atlantic to another, thereby, making the choice for δ a compromise between the dense and sparse areas. This is probably the primary weakness of the use of the multiquadric model. However, provided uniform grid, adequate density and the proper selection of δ, the geoid surface can be measured to a high degree of local detail.

Figures 17 and 18 represent the geoid contours from the reductions utilizing the covariance functions and multiquadric models, respectively. The two contours generally agree to about one to two meters in the very dense portion of the North Atlantic. The less dense portion of the North Atlantic differs by as much as ten meters. When compared to the *Marsh* and *Chang* geometric geoid, it appears that the reduction using the covariance function agrees more favorably, although, the reduction using the multiquadric model showed better agreement in some of the more densely grided areas.

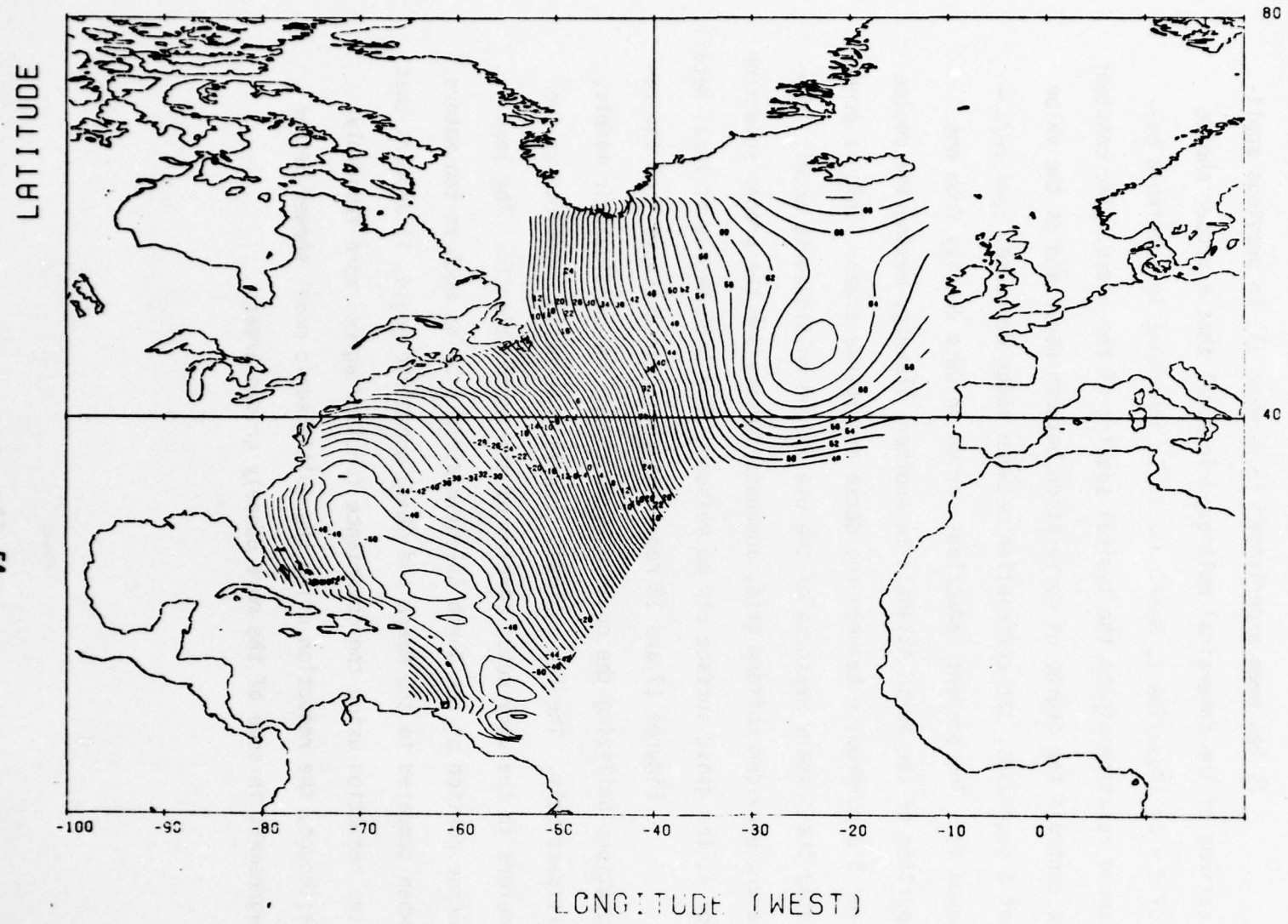

FIGURE 17. Geoid Contour Produced by the Reduction use of the Covariance Function Surface Model

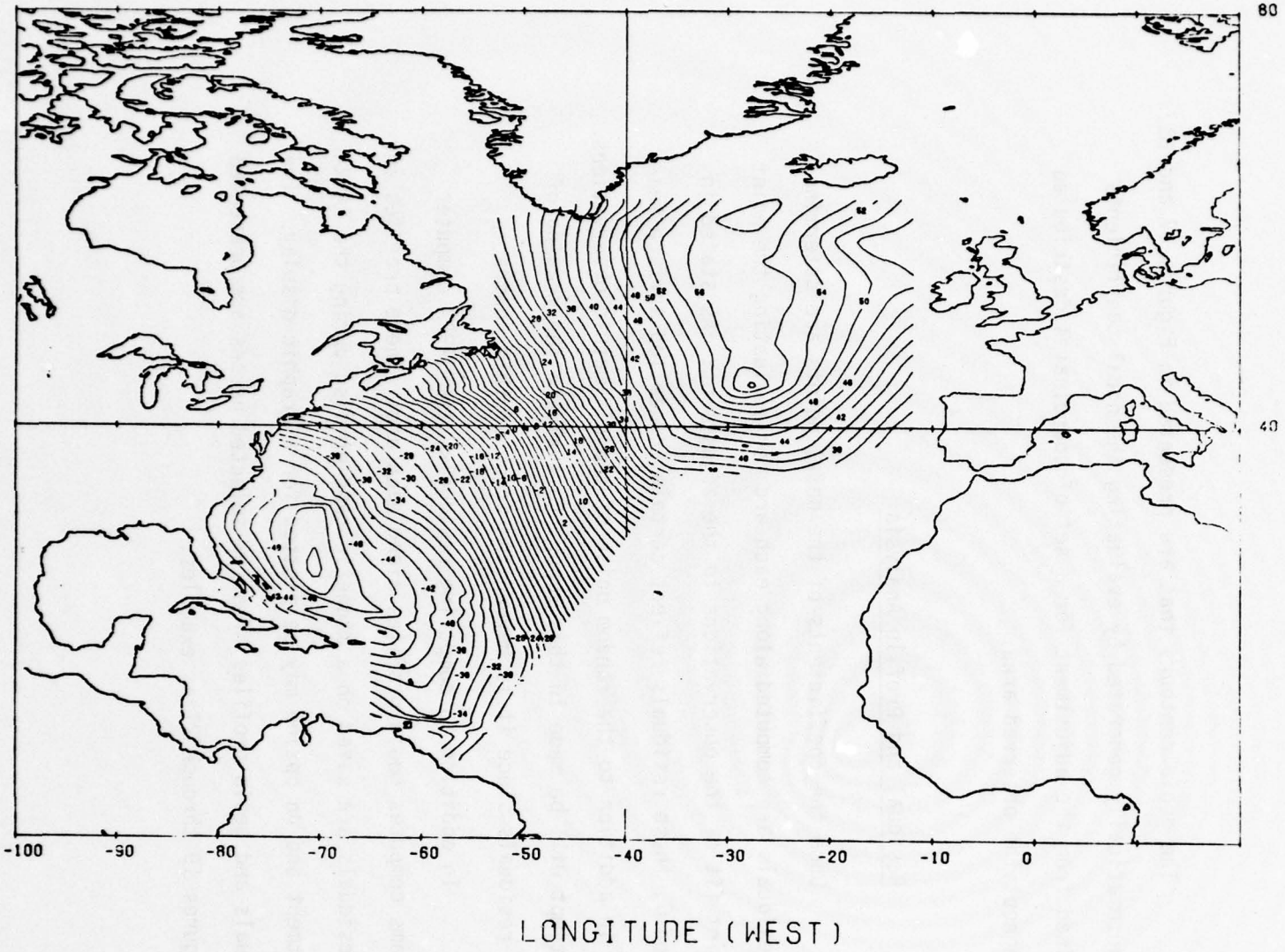

FIGURE 18. Geoid Contour Produced by the Reductions Using the Multiquadric Analysis for the Surface Model

The geoid contours that are presented in Figures 17 and 18, are automatically generated by evaluating the nodal coefficients obtained from the adjustment for a set of coordinates destributed throughout the observed area.

7.3 Residual and Profile Analysis

Once the coefficients of the nodal points are determined, the residuals are computed along each arc for evaluating the point to point fit of the observations to the adjustment. As stated in Section 6, these residuals reflect certain unmodelled surface features in addition to the random noise of the altimetric observations. No attempt will be made in this report to evaluate the meaning of these residuals since it is beyond the scope of this contract.

In addition to computing residuals, the SARRA computer programs computes geoid profiles along each arc. These profiles and the residuals are saved on a magnetic tape or disc during the SARRA adjustment and on option may be plotted for a graphic display. The residuals and geoid profiles of a few selected passes are presented in Figures 19 through 27 as examples.

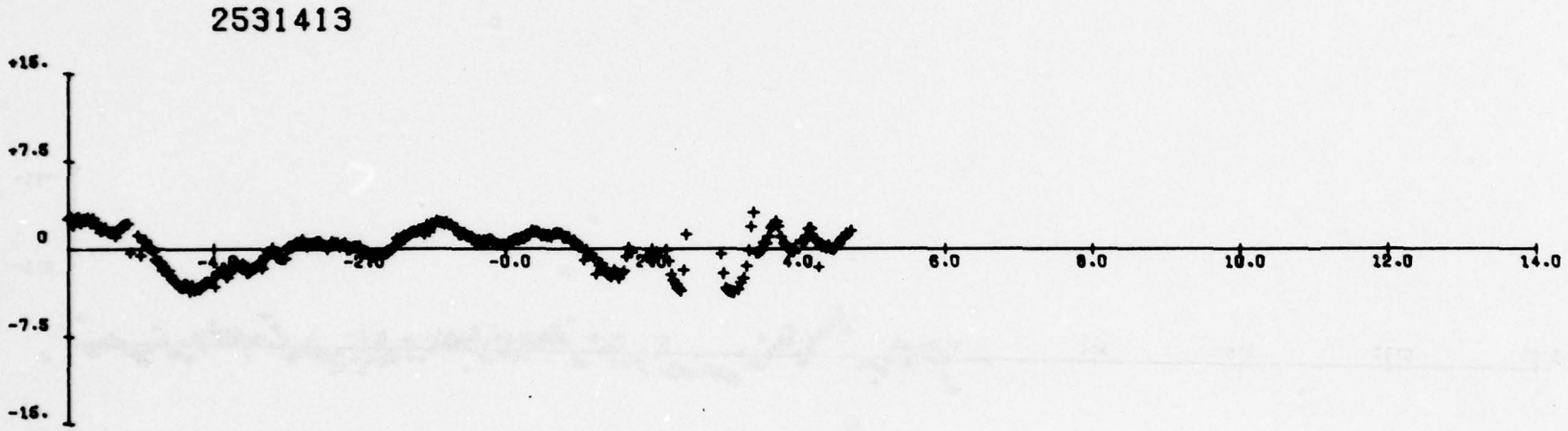

FIGURE 19. Residuals from Pass 2531413

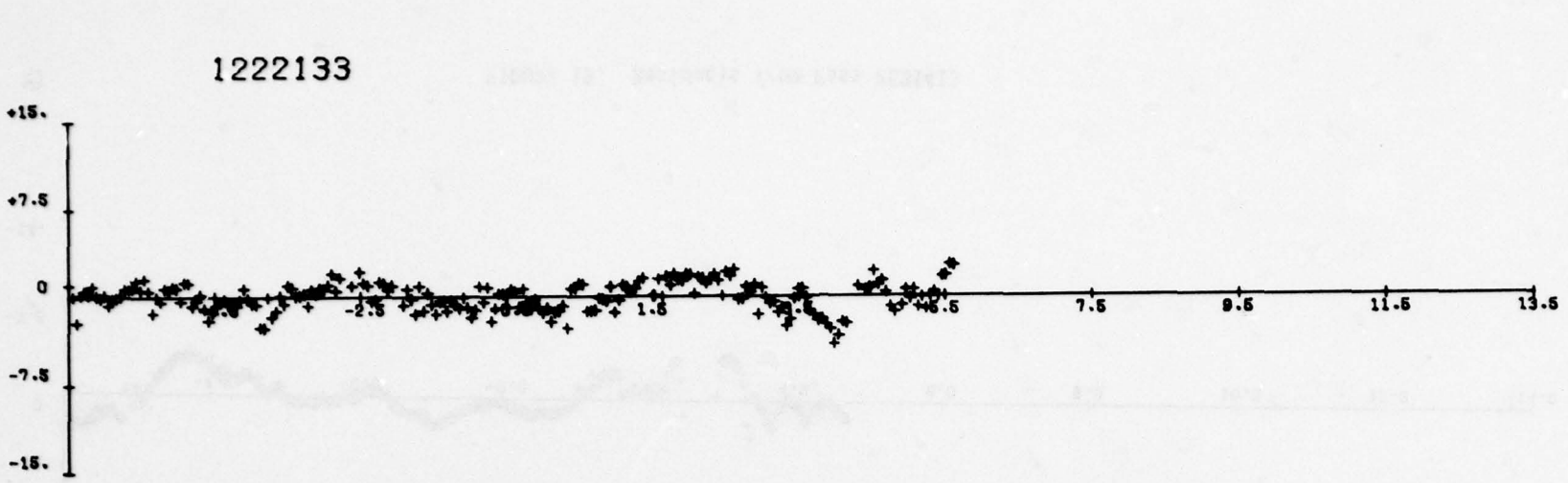

FIGURE 20. Residuals from Pass 1222133

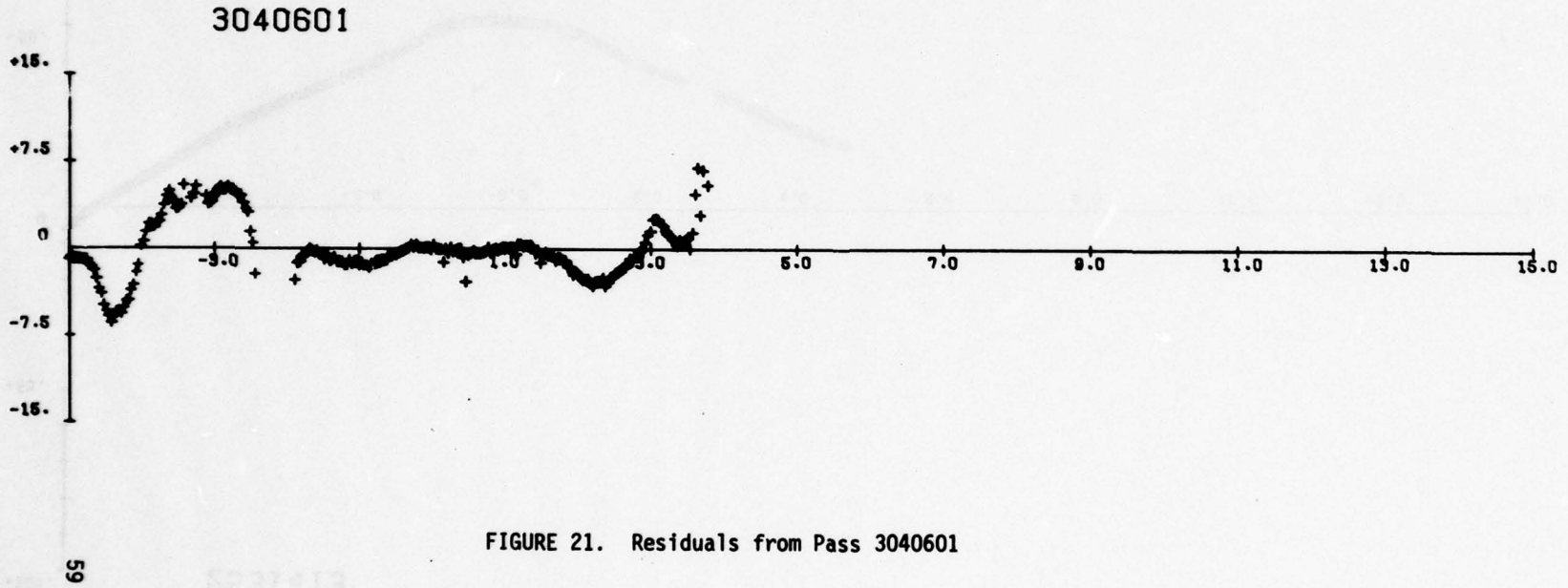

FIGURE 21. Residuals from Pass 3040601

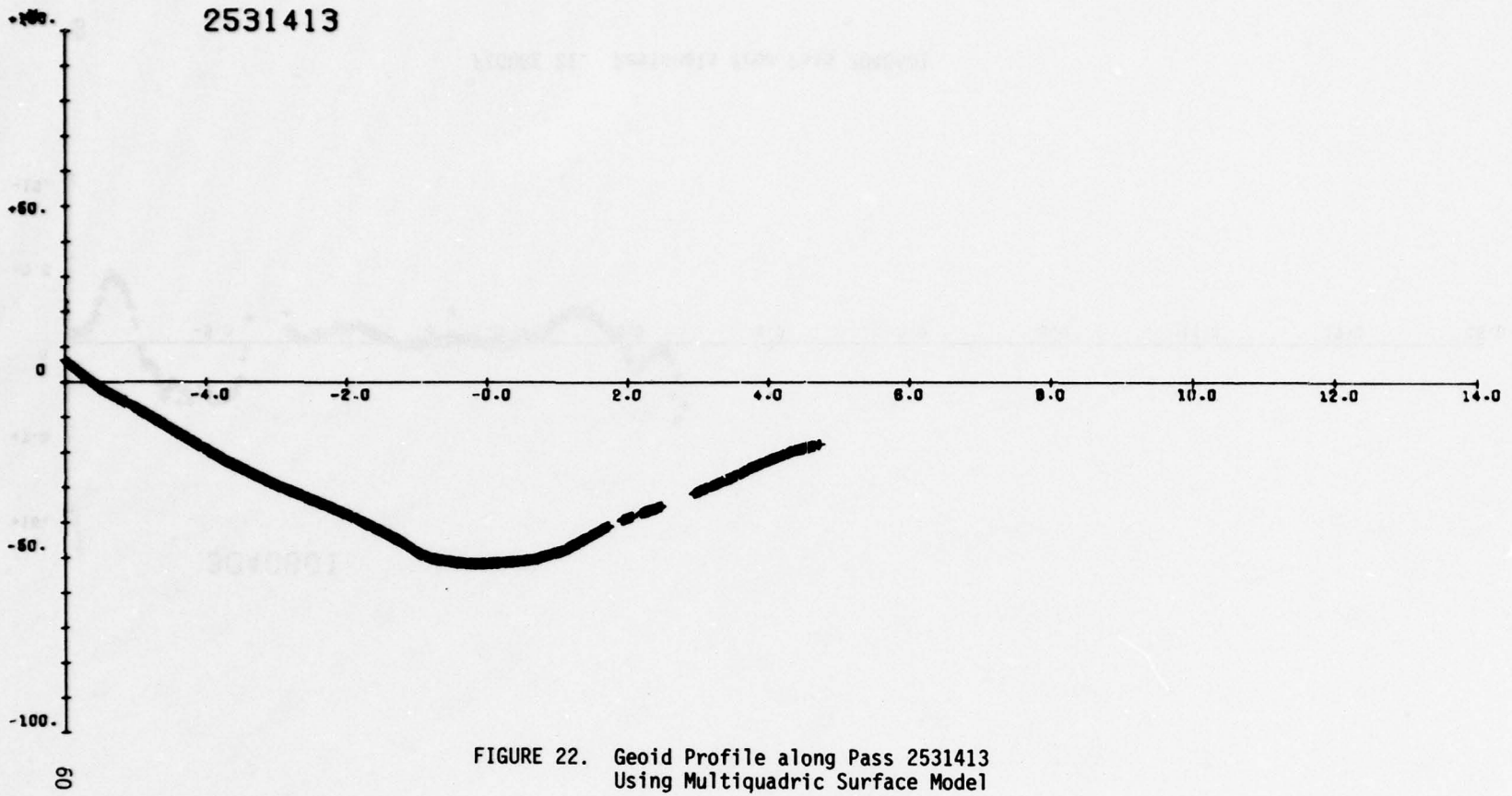

FIGURE 22. Geoid Profile along Pass 2531413
Using Multiquadric Surface Model

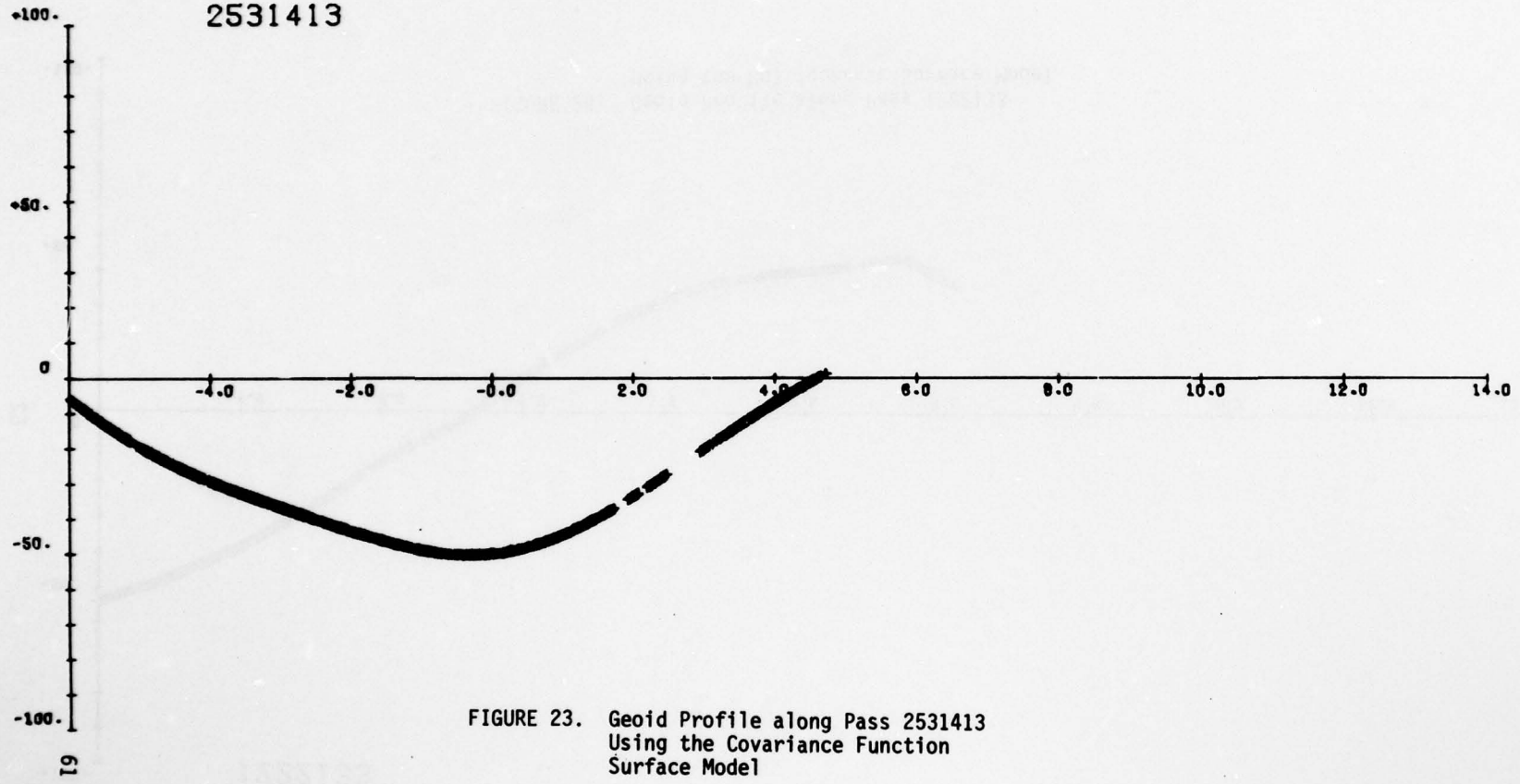

FIGURE 23. Geoid Profile along Pass 2531413 Using the Covariance Function Surface Model

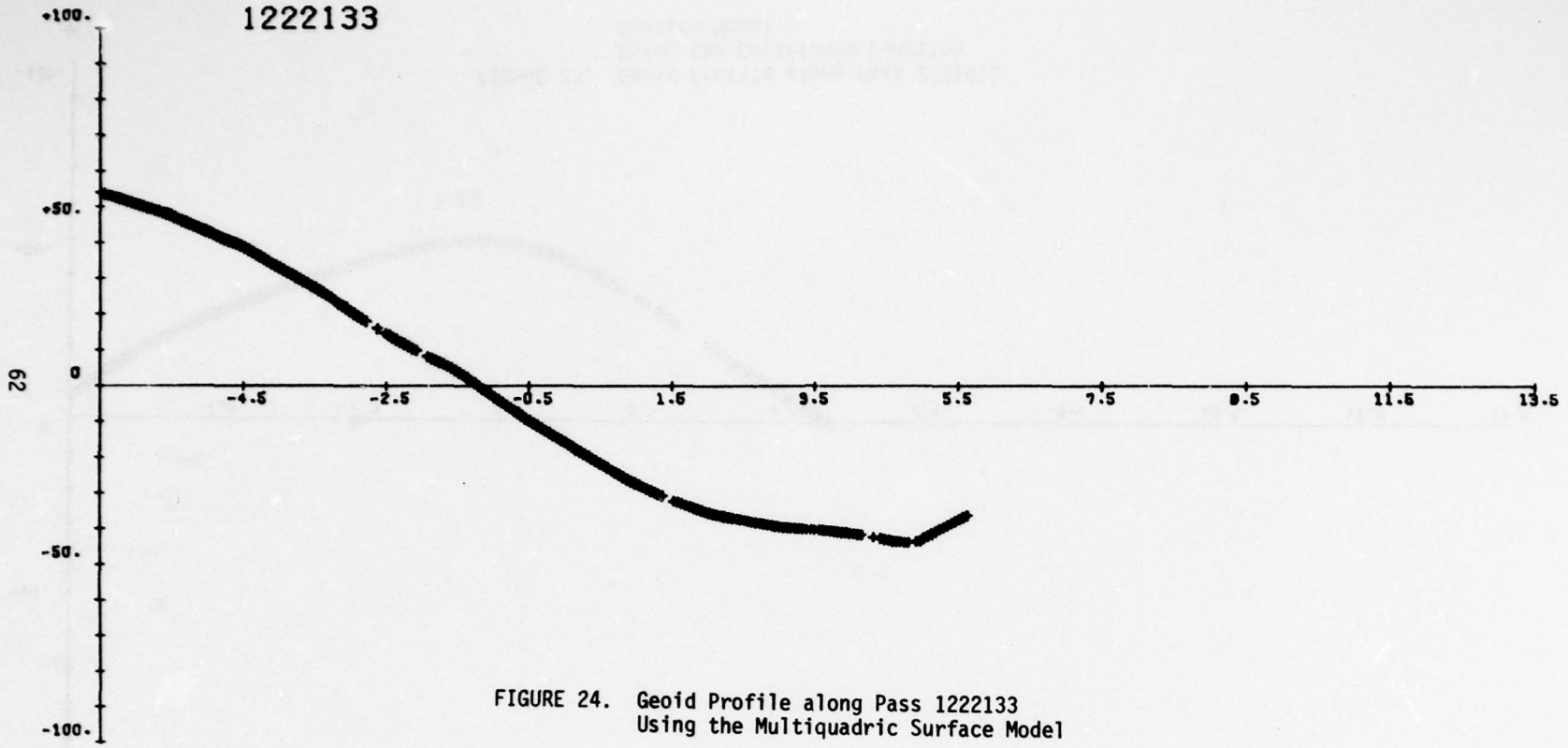

FIGURE 24. Geoid Profile along Pass 1222133
Using the Multiquadric Surface Model

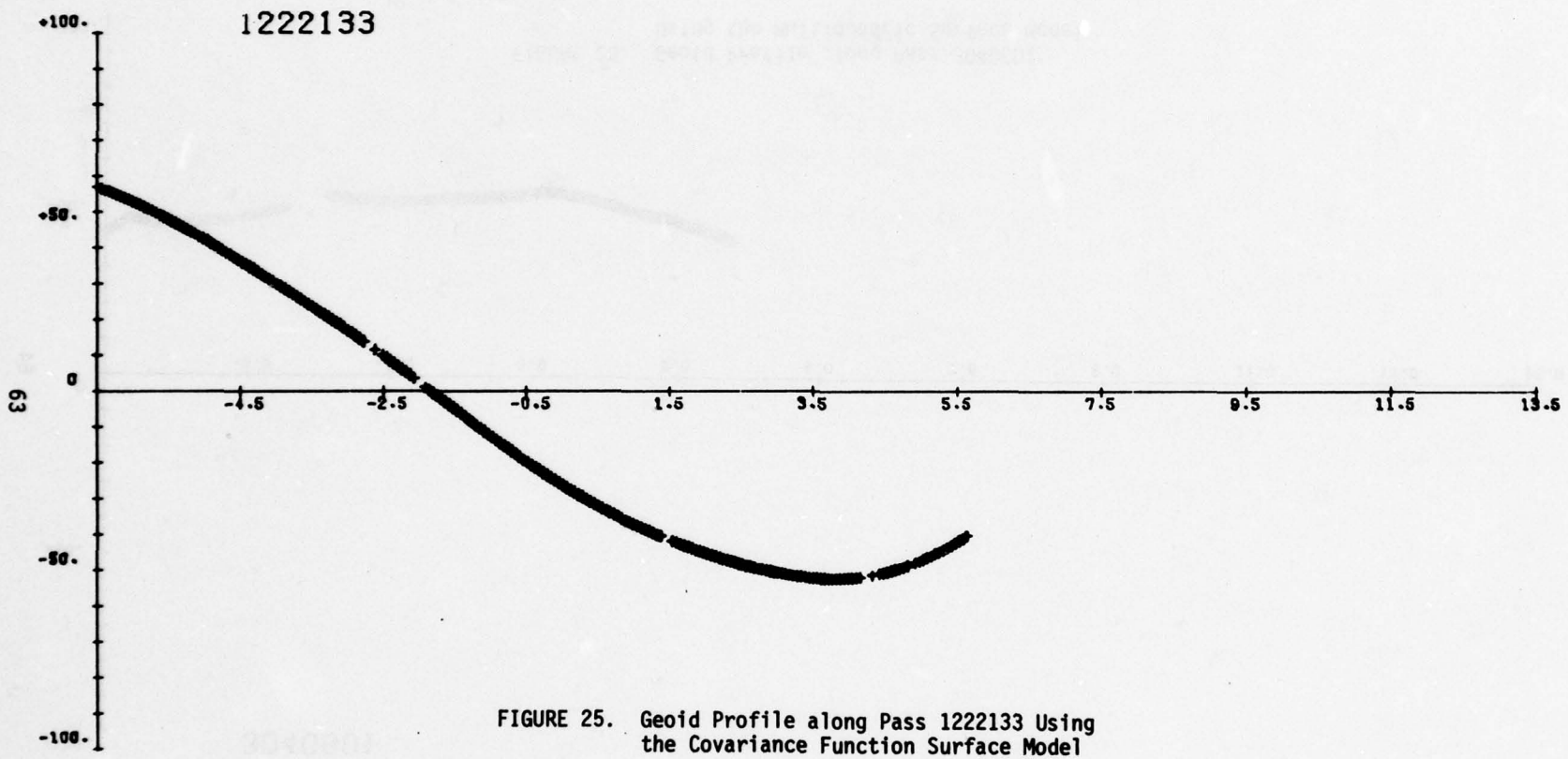

FIGURE 25. Geoid Profile along Pass 1222133 Using the Covariance Function Surface Model

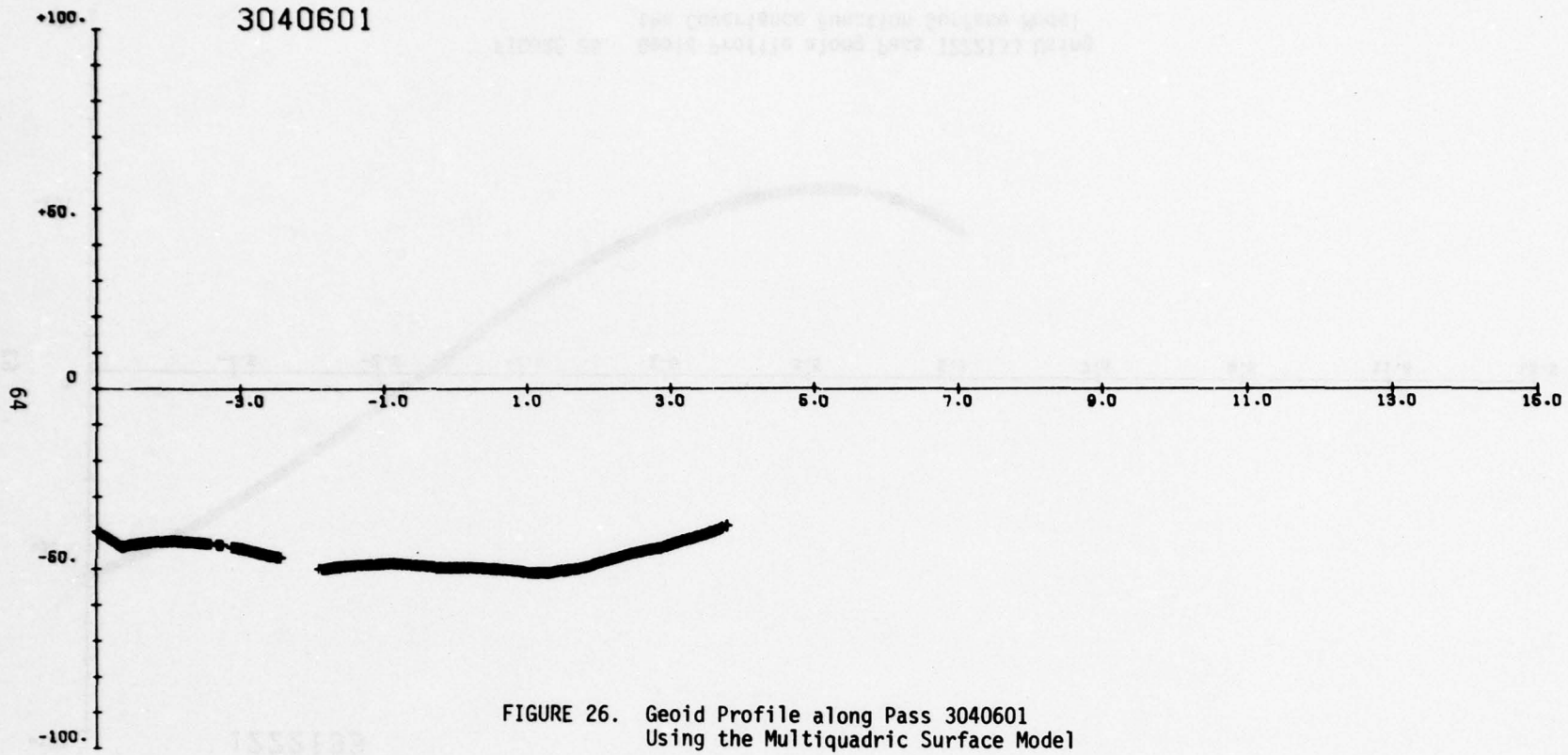

FIGURE 26. Geoid Profile along Pass 3040601
Using the Multiquadric Surface Model

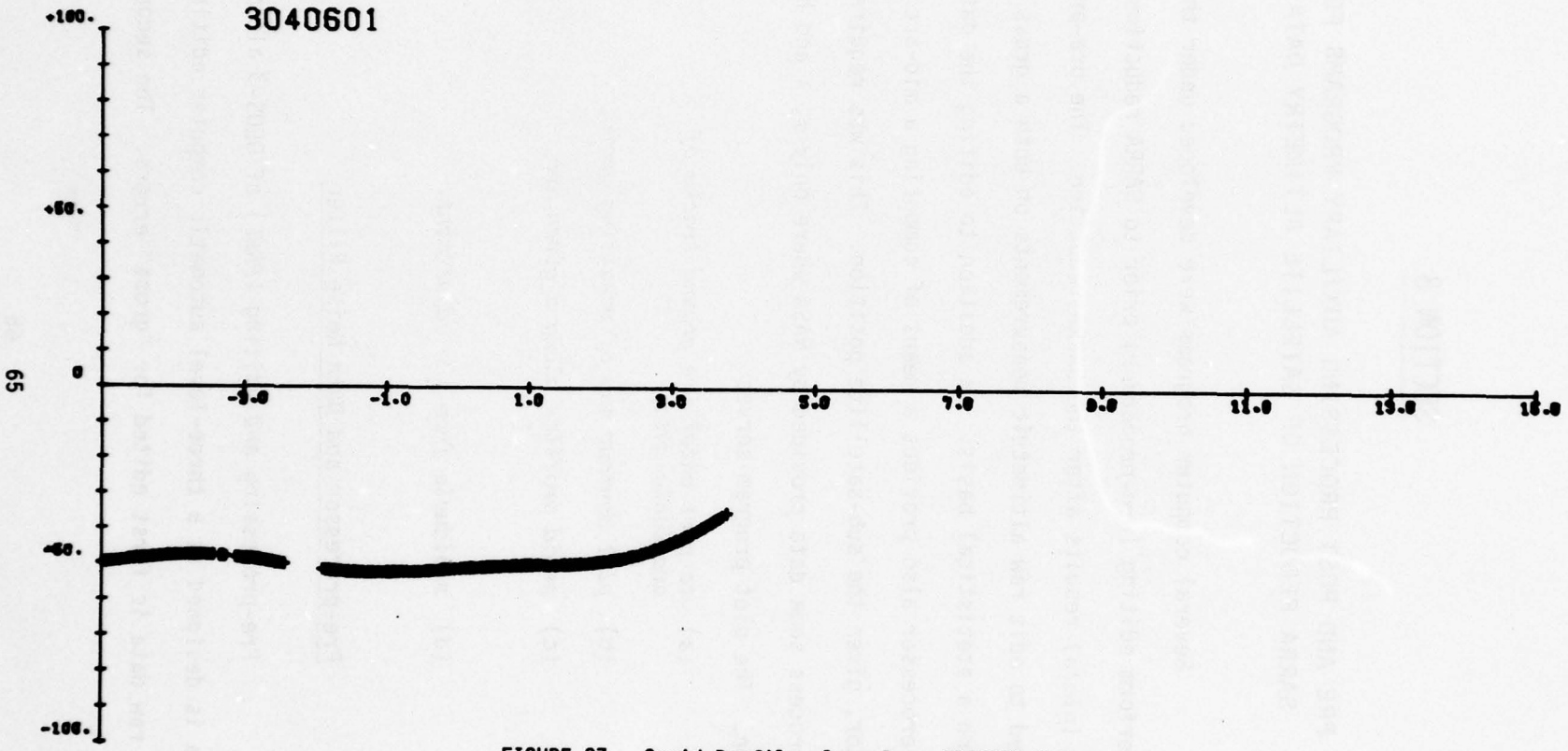

FIGURE 27. Geoid Profile along Pass 3040601 Using the Covariance Function Surface Model

SECTION 8

PRE AND POST PROCESSING AUXILIARY PROGRAMS FOR SARRA REDUCTION OF SATELLITE ALTIMETRY DATA

Several computer programs were developed under this contract to perform editing (*pre-processor*) prior to SARRA reduction and display (*plots*) results after the SARRA reduction. The pre-processor served to edit raw altimetric measurements on both a gross error and on a statistical basis. In addition to editing the data, the pre-processor also provides a means of computing a mid-arc state vector, given the sub-satellite position. This was required to process some data provided by NASA where only ϕ, λ and h were given. The plot program serves

(a) *to plot satellite ground tracks of available data,*

(b) *plot contour map of resulting geoid,*

(c) *geoid profiles along a given arc,*

and

(d) *residuals from the adjustment.*

8.1 Pre-processor and Data Noise Filter

Pre-processing and editing (*PREP*) of GEOS-3 altimetric data is designed as a three-level automatic computer editing effort. The raw data is first edited for "gross" errors. The second step

is to examine the data for continuity and eliminate abrupt changes. The third level of editing rejects data, either smoothed or unsmoothed, that have standard deviations greater than some specified criterion. The editing is accomplished in three steps,

(1) *comparing altimetric measurements with a reasonable expected range of possible heights (h) for gross error such as parity errors;*

(2) *continuity is detected by comparing the change in the measured altimetry (Δh) between successive data points with the corresponding change in time (Δt). This is a measure of the altimetry rate ($\dot{h}$) which is a smooth function. If the altimetry rate exceeds the maximum value, the point is rejected. The maximum for* $\dot{h}$ *may be estimated emperically from several sets of GEOS-C altimetry data.*

(3) *The third level of editing rejects data based upon an input sigma criterion. The criterion will be based upon realistic expected accuracy of the GEOS-3 altimeter measurements.*

The criterion chosen in step 3 should be a little relaxed to make sure that points are not rejected that truly reflect some surface details that are normal sea state variations.

In addition to editing measurement data, the pre-processor can compute a mid-arc state vector when the ephemeris is provided with the altimetric data tape in the form of latitude, longitude and height. The following computational steps are implemented in the pre-processor.

The procedure followed in computing a mid-arc state vector for each pass, was to compute Cartesian coordinates from

the provided geographic coordinates. These coordinates were computed by

$$N = a/(1 - e^2 \sin^2 \phi)^{\frac{1}{2}}$$

$$\begin{bmatrix} X \\ Y \\ Z \end{bmatrix} = \begin{bmatrix} (N+h) \cos \phi \cos \lambda \\ (N+h) \cos \phi \sin \lambda \\ [N(1-e^2) + h] \sin \phi \end{bmatrix}$$

Where a = the earth semi-major axis

e = eccentricity of earth

A fifth order polynomial fit to these coordinates was performed in order to reduce the effect of the above truncation error and to provide a means for computing velocity components.

The general polynomial expression is given by

$$X_i = a_0 + a_1 t_i + a_2 t_i^2 \quad \ldots \quad a_n t_i^n$$

The equation written in matrix form for all i is expressed by:

$$\begin{bmatrix} X_1 \\ X_2 \\ . \\ . \\ . \\ X_i \end{bmatrix} = \begin{bmatrix} 1 \; t_1 t_1^2 \ldots t_1^n \\ 1 \; t_2 t_2^2 \ldots t_2^n \\ . \\ . \\ . \\ 1 \; t_i t_i^2 \ldots t_i^n \end{bmatrix} \cdot \begin{bmatrix} a_0 \\ a_1 \\ . \\ . \\ . \\ a_n \end{bmatrix}$$

Substituting C for the X_i vector, B for the t_i^n matrix and S for the a_i vector, yields

$$C = BS .$$

The least squares solution (*with unit weight matrix*) for the coefficient vector S is

$$S = (B^T B)^{-1} B^T C .$$

The n^{th} order polynomial equation is evaluated at mid-arc time, t_0 where

$$t_0 = (t_i - t_1) / 2 .$$

The velocity component at t_0, $\dot{X}$, is computed from the first derivative of position by

$$\dot{X} = \frac{\partial X_0}{\partial t_0} = a_1 + 2\, a_2 t_0 + 3\, a_3 t_0^2 + n a_n t_0^{n-1} .$$

This procedure is repeated for the Y, $\dot{Y}$ and Z, $\dot{Z}$ components. All altimeter observation times (t_i) are initialized with respect to mid-arc by

$$t_{io} = t_i - t_o .$$

The velocity components corrected for the earth rotation are computed from

$$\begin{aligned} \dot{x}_o &= \dot{X}_0 - \Psi Y_0 \\ \dot{y}_o &= \dot{Y}_0 + \Psi X_0 \\ \dot{z}_o &= \dot{Z}_0 , \end{aligned}$$

to obtain inertial components (Ψ = *earth rotation rate*).

The resulting state vector representing the orbit at mid-arc (X_0, Y_0, Z_0, $\dot{x}_0$, $\dot{y}_0$ and $\dot{z}_0$) is input to the SARRA program with the appropriate constraints.

8.2 Post SARRA Plot Programs

The plot program provides the capability of producing satellite ground track plots, geoid contours and either geoid profiles or residual profiles. Additionally, the land features superimposes on the ground track and the contours. Initially, the land outline was read from maps and input into the program plots. This was later replaced at AFGL by a magnetic tape containing the digitized shoreline coordinates. Each plot is described as follows:

(a) *Ground Track Plot.* *This program plots the ground track of satellite passes over the North Atlantic from a given sub-satellite latitude and longtitude. Additional parallels and meridians may be selected with program input parameters. The ground track plots may be contained within the North Atlantic data boundaries as shown in Figure 28.*

(b) *Contour Plots.* *Contours of either the standard deviations or the actual geoid heights may be plotted. The standard deviations are computed from the covariance matrix from the SARRA reductions. The geoid heights are computed from the surface coefficients saved from the SARRA solution. In either case, the computations are performed for a grid of surface points. The generated grid is contained within the boundaries of the observed geoid and the boundaries of the North Atlantic.*

(c) **Residuals.** *The altimeter observation residuals (measured minus computed height) obtained from the SARRA reductions are plotted for the purpose of visually reviewing measurement characteristics. The residual profile plot provides immediate display of altimeter measurements noise and such oceanic details as sea state variations.*

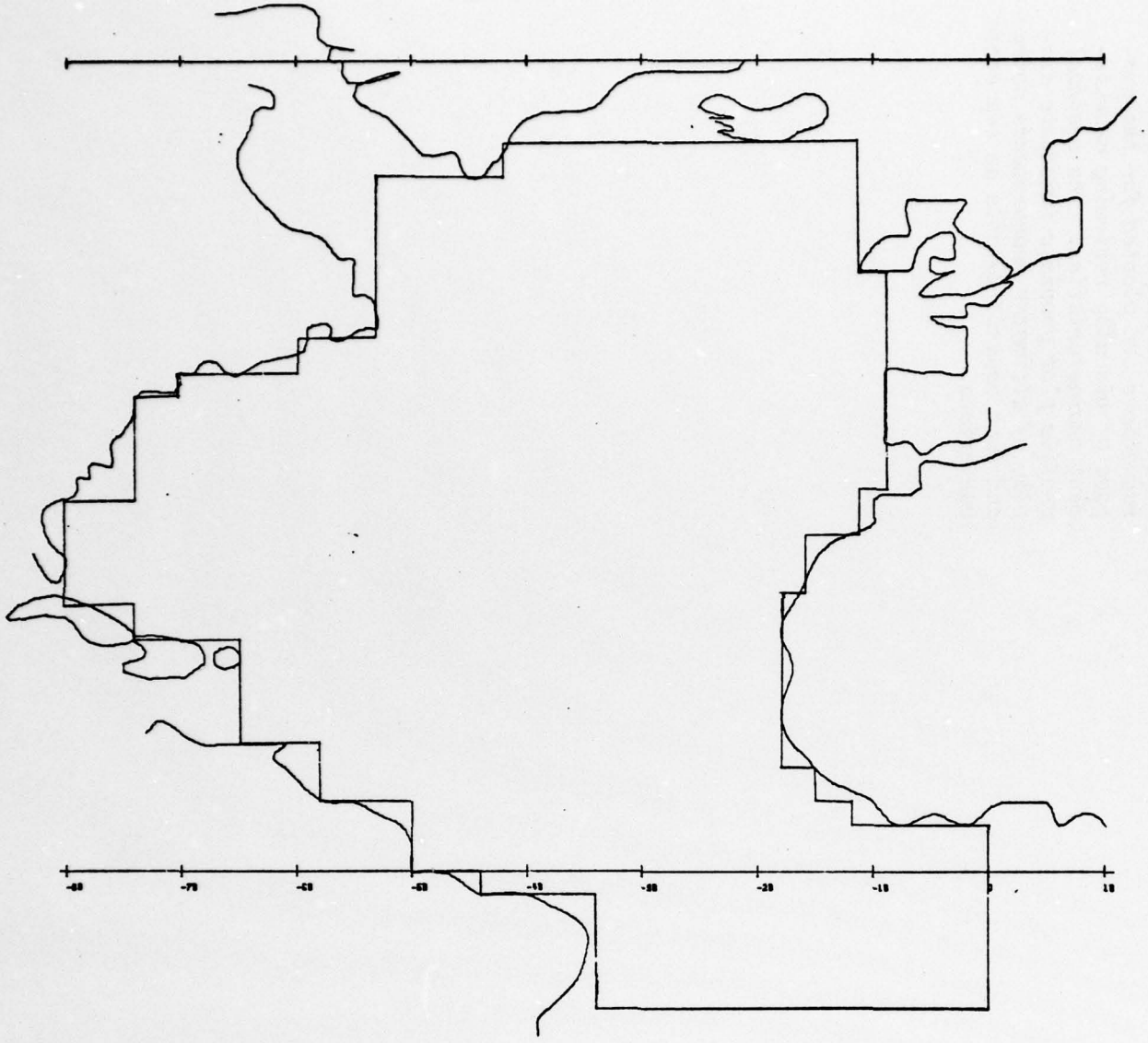

Figure 28. North Atlantic Data Rejection Limits

APPENDIX A

The use of the Covariance Function in the Short Arc Reduction of Radar Altimetry Program

The following derivation of the covariance function and its application to the modelling of geoid surface in the SARRA computer program was developed by Dr. Georges Blaha of DBA Systems, Inc. under a special investigation. The results of Blaha's investigation is reproduced as an appendix for detailed reference material regarding Section 4 of this report.

Covariance Function for Geoid Undulations

The covariance function for geoid undulations (N) is derived from the basic formula

$$N = \frac{R}{\gamma} \sum_{n=2}^{\infty} \frac{1}{n-1} \sum_{m=0}^{n} (\bar{c}_{nm} \cos m\lambda + \bar{d}_{nm} \sin m\lambda) \bar{P}_{nm} (\sin \bar{\varphi}), \qquad (1)$$

where

R - is the mean earth radius ($R \simeq 6371$ km),

γ - is the mean value of gravity ($\gamma \simeq 979.8$ gal),

$\bar{\phi}, \lambda$ - are the geocentric latitude and longitude of the point associated with N:

the other overbars indicate that we are dealing with "fully normalized" harmonics. We have ($m \neq 0$):

$$\bar{P}_{no} (\sin \bar{\varphi}) \equiv \bar{P}_{n} (\sin \bar{\varphi}) = \sqrt{2n+1}\ P_n (\sin \bar{\varphi}),$$

$$\bar{P}_{nm} (\sin \bar{\varphi}) = \sqrt{2\ (2n+1)\ \frac{(n-m)!}{(n+m)!}}\ P_{nm} (\sin \bar{\varphi}),$$

P_n (sin $\bar{\varphi}$) and P_{nm} (sin $\bar{\varphi}$) being called Legendre's polynomials and associated Legendre functions, respectively. Furthermore,

$$\begin{Bmatrix} \bar{c}_{nm} \\ \bar{d}_{nm} \end{Bmatrix} = \gamma\,(n-1) \begin{Bmatrix} \Delta\,\bar{C}_{nm} \\ \Delta\,\bar{S}_{nm} \end{Bmatrix} \qquad (2)$$

where

$$\Delta\,\bar{C}_{no} = \Delta\,C_{no} / \sqrt{2n+1}\,, \qquad (3a)$$

$$\begin{Bmatrix} \Delta\,\bar{C}_{nm} \\ \Delta\,\bar{S}_{nm} \end{Bmatrix} = \sqrt{\frac{1}{2\,(2n+1)} \times \frac{(n+m)!}{(n-m)!}} \begin{Bmatrix} \Delta\,C_{nm} \\ \Delta\,S_{nm} \end{Bmatrix}\,, \qquad (3b)$$

and where

$\Delta\,C_{no}$ - is the correction to the reference C^*_{no} (to be mentioned) in order to obtain C_{no},

$\Delta\,C_{nm} \equiv C_{nm}$,

$\Delta\,S_{nm} \equiv S_{nm}$;

the coefficients C_{no}, C_{nm}, S_{nm} are sometimes called "conventional C's and S's".

It has to be emphasized that equation (1) is valid for the reference ellipsoid having the same mass and the same potential as the geoid. This condition is fulfilled by the "mean earth ellipsoid" which in theory shares with the actual earth two additional parameters (ω = rotation rate and $J_2 = -C_{20}$). The pertinent constants of the mean earth ellipsoid in the Geodetic Reference System (GRS) 1967 are:

$$C^*_{20} = -\,1.0827 \times 10^{-3}, \qquad (4a)$$

$$C^*_{40} = +\,2.37 \times 10^{-6}, \qquad (4b)$$

$$C^*_{60} = -\,6.1 \times 10^{-9}; \qquad (4c)$$

the other C^*_{no} are essentially zero (already C^*_{60} is very small and is sometimes neglected).

In what follows we shall be dealing with overbarred coefficients related to their conventional counterparts by the factors shown in the equations (3). Adopting the mean earth ellipsoid as the reference ellipsoid, we thus have in agreement with the equations (4):

$$\bar{C}^*_{20} = -.484194 \times 10^{-3}, \tag{5a}$$

$$\bar{C}^*_{40} = +.790 \times 10^{-6} \tag{5b}$$

$$\bar{C}^*_{60} = -.17 \times 10^{-8}. \tag{5c}$$

In analogy with previous notations (conventional case), we write

$$\Delta \bar{C}_{20} = \bar{C}_{20} - \bar{C}^*_{20}, \tag{6a}$$

$$\Delta \bar{C}_{40} = \bar{C}_{40} - \bar{C}^*_{40}, \tag{6b}$$

$$\Delta \bar{C}_{60} = \bar{C}_{60} - \bar{C}^*_{60}. \tag{6c}$$

For all the other $\Delta \bar{C}_{nm}$ we have essentially (even if m = 0):

$$\Delta \bar{C}_{nm} \equiv \bar{C}_{nm}; \tag{7a}$$

all $\Delta \bar{S}_{nm}$ are in fact $\bar{S}_{nm}$ themselves, namely

$$\Delta \bar{S}_{nm} \equiv \bar{S}_{nm}. \tag{7b}$$

The covariance function D (ψ) for geoid undulations is obtained by averaging the product N N' over the unit sphere,

$$D(\psi) = M\{N\,N'\}; \tag{8}$$

N and N' in this expression are the geoid undulations at any two points separated by the spherical distance ψ and the symbol M indicates the average over the unit sphere, namely

$$M\{\cdot\} \equiv \frac{1}{4\pi} \iint_{\sigma} (\cdot)\, d\sigma,$$

where σ represents the surface of this sphere and $d\sigma$ is the element of surface area. It can be shown that the covariance function in (8) may be expressed from (1) as follows:

$$D(\psi) = \sum_{n=2}^{\infty} d_n P_n(\cos\psi), \tag{9}$$

where

$$d_n = \frac{R^2}{G^2 (n-1)^2} \sum_{m=0}^{n} (\Delta \bar{C}^2_{nm} + \Delta \bar{S}^2_{nm}); \tag{10}$$

the quantities d_n are called "degree variances" for geoid undulations. If $\psi = 0$, we have from (9):

$$D(0) = \sum_{n=2}^{\infty} d_n. \tag{9'}$$

In the program SARRA, the covariance function serves to express the geoid undulation (N_i) at a geoidal point P_i as a function of parameters c_j at selected nodes P_j:

$$N_i = \sum_{j} D(\psi_{ij})\, c_j, \tag{11}$$

where ψ_{ij} is the spherical distance between P_i and P_j. The overall adjustment model in SARRA can be written as

$$H_i = R_i - r_i + d_i,$$

where

R_i - is the radial distance (from the coordinate origin 0) to the satellite point S_i,

r_i - is the radial distance to the subsatellite point P_i,

H_i - is the satellite altimetry observation (distance $S_i P_i$).

The small unadjustable quantity d_i accounts for the fact that 0, P_i, and S_i do not lie on a straight line; it is not needed explicitly. The parameters c_j from (11) enter into the adjustment process through the model equation

$$r_i = r_i' + N_i,$$

where r_i' is the radial distance to the reference ellipsoid (it is computed from $\bar{\varphi}_i$).* The remaining parameters are the state vector components; these parameters are always weighted. The adjustment model in SARRA may thus be written symbolically as follows:

$$H_i = R_i \text{ (state vector parameters)} - N_i \text{ (c_j parameters)} - r_i' (\bar{\varphi}) + d_i. \quad (12)$$

When performing partial differentiation of this equation with respect to the parameters, it should be kept in mind that $\bar{\varphi}$ in $r_i' (\bar{\varphi})$ depends to a certain extent on the state vector parameters. (See reference 10 for a detailed discussion.)

---

* $r_i' = a/[1 + \frac{e^2}{1-e^2} \sin^2 \bar{\varphi}_i]^{\frac{1}{2}}$, a and e^2 being the usual ellipsoidal parameters

In order to form the observation equations, from (12) we deduce

$$H_i^b + v_i = R_i^o - N_i^o - r_i' + d_i + \frac{\partial (R_i - r_i')}{\partial (\text{state vector par.})_o} \, d\,(\text{state vec. par.})$$
$$- \frac{\partial N_i}{\partial (c_j \text{ par.})_o} \, d\,(c_j \text{ par.}),$$

where v_i is the residual, H_i^b is the observed altimetry and "o" denotes the approximate (initial) values of parameters or functions of such parameters. The state vector parameters are X, Y, Z, $\dot{X}$, $\dot{Y}$, $\dot{Z}$ in the "Earth Fixed" (E.F.) coordinate system; the adjustment in SARRA is effectuated in this system. From (11) we have

$$\frac{\partial N_i}{\partial (c_j \text{ par.})_o} = [D(\psi_{i1}), \ldots, D(\psi_{ij}), \ldots];$$

due to the linearity in (11), one can take

$$c_j^o = 0$$

and thus

$$N_i^o = 0,$$

which is in fact used in SARRA.

The observation equation is then written as follows:

$$v_i = \left\{ -[D(\psi_{i1}), \ldots, D(\psi_{ij}), \ldots] \,\vdots\, + \frac{\partial (R_i - r_i')}{\partial (X, \ldots \dot{Z})_o} \right\} x$$
$$x \begin{bmatrix} dc_1 \\ \vdots \\ dc_j \\ \vdots \\ \hline dX \\ \vdots \\ d\dot{Z} \end{bmatrix} + (R_i^o - r_i' - H_i^b + d_i). \qquad (13)$$

With self-explanatory notations this equation is presented as

$$v_i = a_i \gamma + l_i, \tag{14a}$$

where

$$l_i = r_i^b - r_i', \tag{14b}$$

$$r_i^b \equiv R_i^o - H_i^b + d_i. \tag{14c}$$

The term l_i is sometimes called "discrepancy term". The quantity r_i^b can either be computed as in (14c), or it can be computed as the distance $\overline{OP_i}$ from the coordinates of the point P_i depicted in Figure 1. This is in fact the procedure used in SARRA.

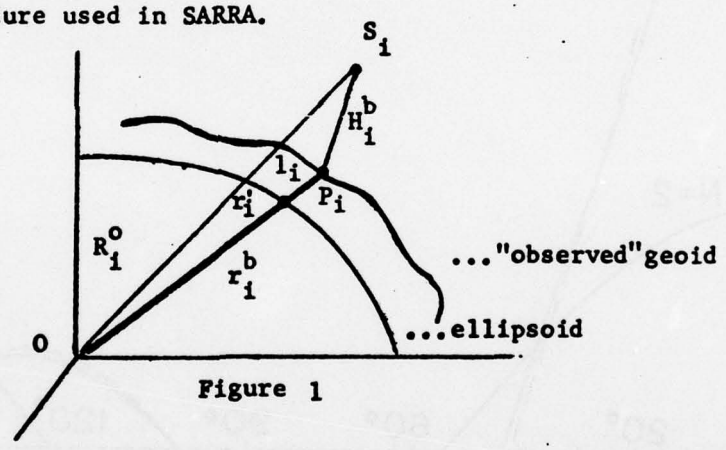

Figure 1

By joining together individual observation equations along one short arc, the resulting set can be written in matrix notations as follows:

$$V = A\chi + L.$$

Similar procedure would apply for other arcs in an adjustment; each vector χ would now contain a different set of state vector parameters (besides the common set of c_j parameters). All these sets would finally be joined

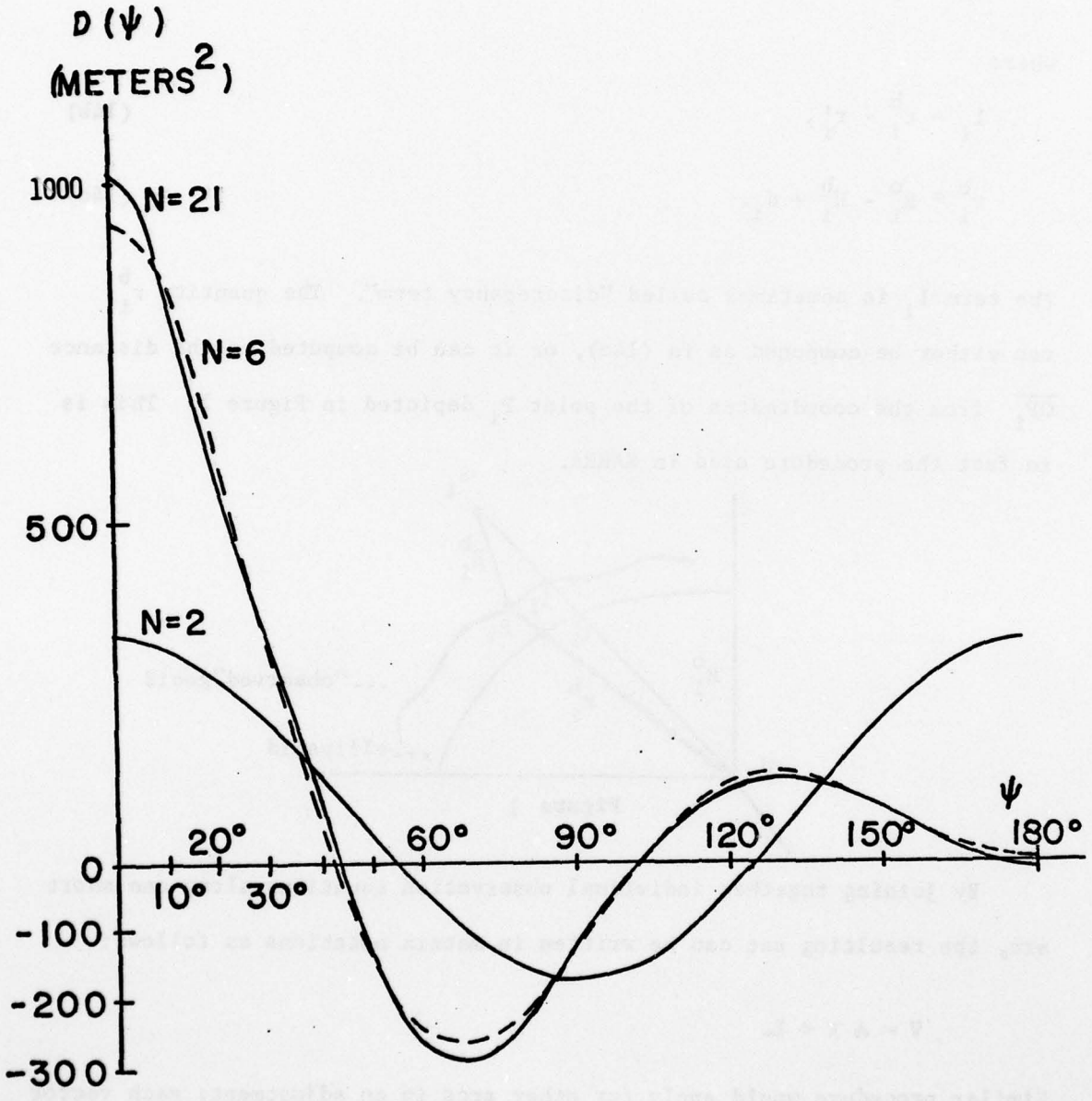

FIGURE 2: COVARIANCE FUNCTION FOR GEOID UNDULATIONS ASSOCIATED WITH DEGREES TRUNCATION N=2, N=6, AND N=21

into one large system of observation equations, and adjusted. However, the main purpose of this brief exposition of the SARRA adjustment model has been to show the role of the covariance function D (ψ). We have seen how to compute this function from potential coefficients. We shall next discuss some practical problems associated with its application.

If a set of potential coefficients ($\bar{C}$'s and $\bar{S}$'s) is given complete through a certain degree n = N, the covariance function D (ψ) may be constructed for varying values ψ (between 0 and 2π) according to the equations (9'), (9). In fact, Figure 2 depicts three cases of the covariance function D (ψ); they correspond to the truncations N = 2, N = 6, and N = 21, associated with a reasonable set of coefficients complete through the degree and order (21,21). The figure reveals that the greatest contribution to the value of the covariance function comes from the lower degree and order coefficients; there is a small difference between D (ψ) for N = 6 and N = 21 and there would be practically no difference if N = 15 and N = 21 were considered. On the other hand, it appears that if, for example, a given (6,6) model were to replace the reference ellipsoid, the corresponding covariance function of new "undulations" would exhibit sharp and distinct features which would vary substantially for different degrees of truncation (up to a relatively large n = N). It is felt that such an approach would be much more sensitive to local geoidal features than is the use of the covariance function D (ψ). In contrast to using D (ψ), such a "modified covariance function" would greatly reduce the influence of distant nodal points (e.g. when $\psi > 30°$) on the value of the "undulation" at observation points.

REFERENCES

1. BROWN, D.C., 1973. Determination of Oceanic Geoid from Short Arc Reduction of Satellite Altimetry. Paper presented to *The First International Symposium: The Use of Artificial Satellites For Geodesy And Geodynamics*, Athens, May 14 - 21, 1973.

2. BROWN, D.C., and TROTTER, J. E., 1969. *SAGA, A Computer Program For Short Arc Geodetic Adjustment of Satellite Observations.* AFCRL Report Number 69-0080, Air Force Cambridge Research Laboratories, Bedford, Massachusetts.

3. HARDY, R. L., 1972. *The Analytical Geometry of Topographic Surfaces.* Proceedings of the 32nd Annual Meeting of The American Congress on Surveying and Mapping, Washington, D.C., March 12-17, 1972. Pages 163 - 181.

4. HARTWELL, J. G., 1968. *A Power Series Solution for the Motion of An Artificial Satellite and Its Concomitant Variational Equations.* DBA Systems, Inc. report presented to Special Projects Branch, *Seventh Astrodynamics Conference*, Goddard Space Flight Center, April, 1968.

5. VINCENT, S.A., STRANGE, W.E., and MARSH, J.G., 1972. *A Detailed Gravimetric Geoid from North America to Eurasic.* NASA GSFC Document X-553-/2-94.

6. MARSH, J.G., CHANG, E.S., 1976. *Detailed Gravimetric Geoid Computations in North America.* Presented at the XIX Meeting of COSPAR, Philadelphia, Pa., June 14 - 19, 1976.

7. HEISKANEN, W.A., MORITZ, H., 1967. PHYSICAL GEODESY, W. H. Freeman and Co., San Francisco, 1967.

8. KAHN, BROWN, CEBOLA, FURY, 1972. *Orbit Accuracy Requirements for Geoid Improvement Using Radar Altimetry* from GEOS-C.

9. HADGIGEORGE, TROTTER, 1976. *Short Arc Reduction of GEOS-3 Altimetric Data.* Presented to American Geophysical Union (AGU), December, 1976.

AFGL-TR-77-0170

1. Report No.	2. Government Accession No.	3. Recipient's Catalog No.
NASA CR-141434		

4. Title and Subtitle	5. Report Date
SHORT ARC REDUCTION OF RADAR ALTIMETRY COMPUTER PROGRAM	January 1978
	6. Performing Organization Code

7. Author(s)	8. Performing Organization Report No.
George Hadgigeorge, Jerry Trotter	

9. Performing Organization Name and Address	10. Work Unit No.
Air Force Geophysics Laboratory Air Force Systems Command United States Air Force Hanscom, AFB, Massachusetts 01731	760003AH
	11. Contract or Grant No. P57,270(G)
	13. Type of Report and Period Covered

12. Sponsoring Agency Name and Address	13. Type of Report and Period Covered
National Aeronautics and Space Administration Wallops Flight Center Wallops Island, Virginia 23337	Final Report, 9/75 - 7/77
	14. Sponsoring Agency Code

15. Supplementary Notes

16. Abstract

The Air Force Geophysics Laboratory computer program SARRA (Short Arc Reduction of Radar Altimetry) has been used for geoid determination with altimetric observations from the GEOS-3 satellite. An important feature of SARRA is the simultaneous recovery of the orbit parameters and the surface coefficients as defined by covariance function weights. Orbits good to approximately 20 meters are adequate for precise geoid determinations by virture of the orbital adjustment in the reductions. Altimetric data over a portion of the North Atlantic Ocean have been processed to derive the regional geoid and gravity field. Analyses of altimeter residuals resulting from the short arc adjustment show that the residuals can be used to define the neglected higher order geoidal undulations with high fidelity and continuity.

17. Key Words (Suggested by Author(s))	18. Distribution Statement
geoid orbit parameters altimeter gravity	Unclassified - unlimited STAR Category - 61

DISTRIBUTION STATEMENT A
Approved for public release;
Distribution Unlimited

19. Security Classif. (of this report)	20. Security Classif. (of this page)	21. No. of Pages	22. Price*
Unclassified	Unclassified	87	

*For sale by the National Technical Information Service, Springfield, Virginia 22151